AD-A189 279 MODULATABLE THIN FILM FIELD EMISSION SPACE GUN(U) STAR 1/1
MICROWAVE CAMPBELL CA R M PHILLIP NOV 87
RADC-TR-87-41 F19628-85-C-0088

UNCLASSIFIED F/G 19/12 NL

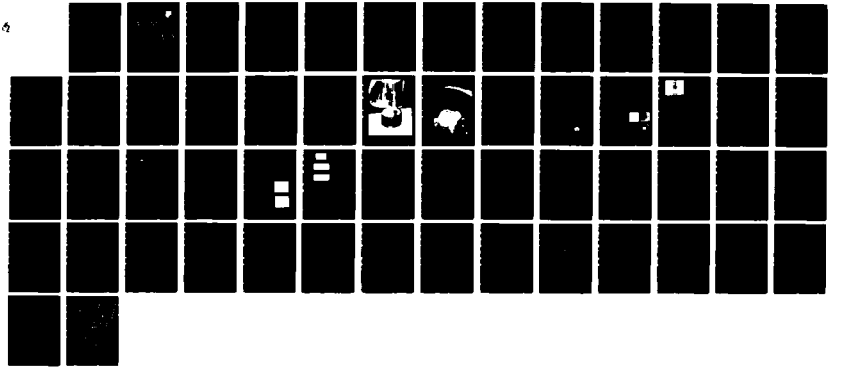

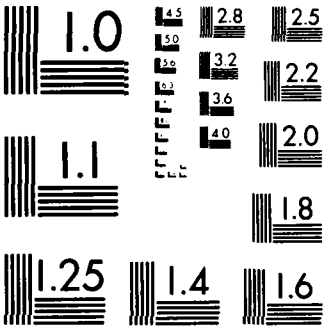

RADC-TR-87-41
Final Technical Report
November 1987

MODULATABLE THIN FILM FIELD EMISSION SPACE GUN

STAR Microwave

Robert M. Phillips

ROME AIR DEVELOPMENT CENTER
Air Force Systems Command
Griffiss Air Force Base, NY 13441-5700

This report has been reviewed by the RADC Public Affairs Office (PA) and is releasable to the National Technical Information Service (NTIS). At NTIS it will be releasable to the general public, including foreign nations.

RADC-TR-87-41 has been reviewed and is approved for publication.

APPROVED:

DALLAS T. HAYES
Project Engineer

APPROVED:

ALLAN C. SCHELL
Director of Electromagnetics

FOR THE COMMANDER:

JOHN A. RITZ
Directorate of Plans & Programs

If your address has changed or if you wish to be removed from the RADC mailing list, or if the addressee is no longer employed by your organization, please notify RADC (EECP) Hanscom AFB MA 01731-5000. This will assist us in maintaining a current mailing list.

Do not return copies of this report unless contractual obligations or notices on a specific document require that it be returned.

UNCLASSIFIED
SECURITY CLASSIFICATION OF THIS PAGE

REPORT DOCUMENTATION PAGE

1a. REPORT SECURITY CLASSIFICATION UNCLASSIFIED	1b. RESTRICTIVE MARKINGS N/A
2a. SECURITY CLASSIFICATION AUTHORITY N/A	3. DISTRIBUTION / AVAILABILITY OF REPORT Approved for public release; distribution unlimited.
2b. DECLASSIFICATION / DOWNGRADING SCHEDULE N/A	
4. PERFORMING ORGANIZATION REPORT NUMBER(S) N/A	5. MONITORING ORGANIZATION REPORT NUMBER(S) RADC-TR-87-41
6a. NAME OF PERFORMING ORGANIZATION STAR Microwave 6b. OFFICE SYMBOL (If applicable)	7a. NAME OF MONITORING ORGANIZATION Rome Air Development Center (EECP)
6c. ADDRESS (City, State, and ZIP Code) 546 Division Street Campbell CA 95008	7b. ADDRESS (City, State, and ZIP Code) Hanscom AFB MA 01731-5000
8a. NAME OF FUNDING / SPONSORING ORGANIZATION Rome Air Development Center 8b. OFFICE SYMBOL (If applicable) EECP	9. PROCUREMENT INSTRUMENT IDENTIFICATION NUMBER F19628-85-C-0088
8c. ADDRESS (City, State, and ZIP Code) Hanscom AFB MA 01731-5000	10. SOURCE OF FUNDING NUMBERS PROGRAM ELEMENT NO. 65502F; PROJECT NO. 3005; TASK NO. RA; WORK UNIT ACCESSION NO 24

11. TITLE (Include Security Classification)
MODULATABLE THIN FILM FIELD EMISSION SPACE GUN

12. PERSONAL AUTHOR(S)
Robert M. Phillips

13a. TYPE OF REPORT	13b. TIME COVERED	14. DATE OF REPORT (Year, Month, Day)	15. PAGE COUNT
Final	FROM Oct 85 TO Jun 86	November 1987	58

16. SUPPLEMENTARY NOTATION
N/A

17 COSATI CODES			18. SUBJECT TERMS (Continue on reverse if necessary and identify by block number)
FIELD	GROUP	SUB-GROUP	Electron Gun; Field Effect Cathode; Electron Source; Thin Film Field Emitter; Modulation
17	02		
20	14		

19. ABSTRACT (Continue on reverse if necessary and identify by block number)

The objective of this research program was to determine the feasibility of using a Spindt type thin film emitter chip to produce amperes of low voltage modulated current at tens of kilovolt beam voltage for a space application. The specific requirement was for a pulse modulated column of electrons of 10 amperes current at 50 kilovolts voltage. A design effort determined that a 2-inch diameter chip would be required to provide this current with conservative emission current density. A conceptual design was developed consisting of an array of emitting regions producing beamlets which were to be accelerated through a gridded or perforated anode at approximately 3 kilovolt voltage, followed by post-acceleration to 50 kilovolts. Feasibility was to be demonstrated by using a smaller (1/2-inch square) standard emitter chip of the type produced by SRI International for their field emissions research program. This chip was to be tested to the same current density as would be required of the 2-inch chip.

A test electron gun employing a standard emitter chip was designed and fabricated based on the results of a computer-derive electron optics model. Of five emitter chips started by

20. DISTRIBUTION / AVAILABILITY OF ABSTRACT ☐ UNCLASSIFIED/UNLIMITED ☒ SAME AS RPT ☐ OTIC USERS	21. ABSTRACT SECURITY CLASSIFICATION UNCLASSIFIED
22a. NAME OF RESPONSIBLE INDIVIDUAL Dallas T. Hayes	22b. TELEPHONE (Include Area Code) (617) 377-4264 22c. OFFICE SYMBOL RADC (EECP)

DD FORM 1473, 84 MAR 83 APR edition may be used until exhausted. All other editions are obsolete.

SECURITY CLASSIFICATION OF THIS PAGE
UNCLASSIFIED

Block 19 (Cont'd)

SRI Internationa, two were successful and were delivered for use in the test gun. One chip was lost during assembly of the test gun due to breakdown of the chip, apparently from RF leakage while a welding process was being performed. After modifying the construction procedure, the test gun was successfully assembled. However, during tests this chip failed catastrophically at one percent of the current emission which was required to demonstrate feasibility of the approach.

Although it is certain that refinement of the fabrication and handling procedures, which would come with experience, would produce improved results, i.e., higher emission current and reduced gate current, the difficulties encountered to date suggest strongly that the state-of-the-art in the fabrication and use of thin film field emitters is not sufficiently advanced to reliably produce the required 10 amperes of modulatable current. The difficulties involved in getting even one percent of the rated current density from the feasibility model casts grave doubts about using the technique in the near term for producing 16 times higher current (1600 times higher than that observed prior to catastrophic failure of the chip). Recommendations for further research in this area are included in this report.

1.0 SUMMARY AND CONCLUSIONS

1.1 Objective

The objective of this research program was to determine the feasibility of using a Spindt type thin film field emitter to produce amperes of low voltage modulated current at tens of kv beam voltage for a space application. The specific requirement was for a pulse modulated column of electrons of 10 amperes current at 50 kv beam voltage.

The thin film field emitter has two attributes which make it ideal for this application.

1) The total gate voltage with respect to cathode required to obtain the necessary current, even at 50 kv accelerating voltage, is approximately 100 volts and the on/off voltage swing can be as little as 25 or 30 volts.

2) The thin film field emitter requires no heater power.

The unknowns which were to be examined in this first phase of the two-phase research program were:

1) Is the thin film field emitter capable of producing the required 10 amperes of total current? This type of emitter has successfully produced extremely high current densities (up to 100 amperes/cm^2), but always from small emitters which produced milliamperes of total current.

2) Is such a device reliable and rugged enough to stand the rigors of application in close proximity to a space vehicle with its many sources of contamination?

1.2 Approach

A pre-Contract design effort determined that a 2-inch diameter emitting chip would be required to provide 10 amperes of current with conservative emission current density. A conceptual design was developed consisting of an array of emitting regions,

producing beamlets which were to be accelerated through a gridded or perforated anode at approximately 3 kv voltage, followed by post acceleration to 50 kv. Feasibility was to be demonstrated by using a smaller (1/2-inch by 1/2-inch) standard emitter chip of the type produced by SRI International for their field emission research program. This chip, which contains a square array of 21 emitters was to be tested to the same current density per emitter as would be required of the Phase 2 chip. The latter would have 16 times more emitters in its 2-inch diameter. The program was made up of the following tasks:

1) Electron Optics: It is important that essentially all of the current from the field emitter pass through the perforated anode to prevent back bombardment of the emitter by ions produced by interception on the anode. This requires that the emitter diameter, center-to-center spacing, cathode-anode spacing and size of the openings in the perforated anode be properly designed. An analytical solution to the beam trajectory problem was used to develop a model which was then analyzed in greater detail using a numerical solution and a computer code.

2) Using the computer-derived optics, a gun tester was designed and developed which provided for the mounting of the emitter chip in a ceramic pellet which provided the proper registry of the electrodes. The appropriate voltages were applied through a high voltage header.

3) Emitter chips were fabricated and pretested by SRI International, then transported fully mounted in the ceramic pellet. This pellet was transferred to the gun tester at STAR Microwave for final processing and evaluation at high current.

1.3 Results

The test vehicle, which was based on the results of the computer-derived electron optics model, was designed and fabricated on schedule. Out of five emitter chip starts, two were delivered to STAR Microwave. One of these made it to hot test. The other was lost due to breakdown of the chip, apparently from RF leakage in the gun tester welding process. The second chip,

which made it to final test, failed catastrophically at one percent of the current emission which was required to demonstrate feasibility of the approach.

1.4 Conclusions and Recommendations

Although it is certain that refinement of the fabrication and handling procedures, which would come with experience, would produce improved results, i.e., higher emission current and reduced gate current, the difficulties encountered to date suggest strongly that the state-of-the-art in the fabrication and use of thin film field emitters is not sufficiently advanced to reliably produce the required 10 amperes of modulatable current. The difficulties involved in getting even one percent of the rated current density from the feasibility model casts grave doubts about using the technique in the near term for producing 16 times higher current (1600 times higher than that observed prior to catastrophic failure of the chip).

If the research effort is continued, it is recommended that the following investigations and changes in procedure be implemented:

1. Each of the emitters which went through preliminary test at SRI International, and the emitter which started through final test at STAR Microwave, were plagued by excessive gate current. The source of this current needs to be identified and eliminated.

2. Once assembled, baked out and evacuated, the emitter should be subjected to all of the tests, both preliminary and final, without being removed from its original enclosure. The risk of contamination in opening a preliminary test container and transferring the pellet to the space gun tester is too great.

3. Careful analysis should be made of the environment in which the thin film field emitter is to be used in space. Deterioration in the vacuum from the -8 scale to the -6 scale, as indicated by the ion pump current, resulted in significant deterioration in the emission of the chip at STAR Microwave An equivalent poor vacuum in space could produce equal or greater performance deterioration.

1.5 Organization of the Report

Section 2 is the description of the experimental test vehicle, the tests which were to be performed, the problems encountered and the test results. Appendix 1 is a more detailed description of the theory and construction of the Spindt thin film field emitter. Appendix 2 presents the analysis and results of the computer study which were used to design the electron optics of the space gun.

2.0 INVESTIGATION OF FIELD EMISSION SPACE GUN

2.1 Design of Space Gun

Figure 1 is a schematic drawing of the proposed Phase II 50 kv, 10 amp space gun with its 2-inch diameter thin film emitting chip. Figure 2 shows details of the emitter geometry, i.e., center-to-center spacing, of the emitting areas and the cathode-to-perforated anode spacing, as determined by the computer study (see Appendix 2). From the computer study it was learned that an anode hole diameter of approximately .080 inches would be required to obtain essentially 100% transmission of the current from the .040 (1 mm) emission areas at a cathode-to-anode spacing of .040 inches.

The .040 inch cathode-to-anode spacing was chosen as the minimum practical spacing for 3 kv accelerating voltage between the cathode and the anode. The required 80 mil holes in the perforated anode leave only a 20 mil web between holes, if the center-to-center spacing of the 1 mm emitting areas is .1 inches. This is the spacing which is used in the standard SRI International 1/2-inch by 1/2-inch chip. From this we concluded that the density of the emitters could not be significantly increased above that already used by SRI International in making its emitting chips. Hence the density, diameter and spacing of emitters was to be the same for the Phase II two-inch diameter emitter as it was for the Phase I 1/2-inch by 1/2-inch emitter. For 10 amps

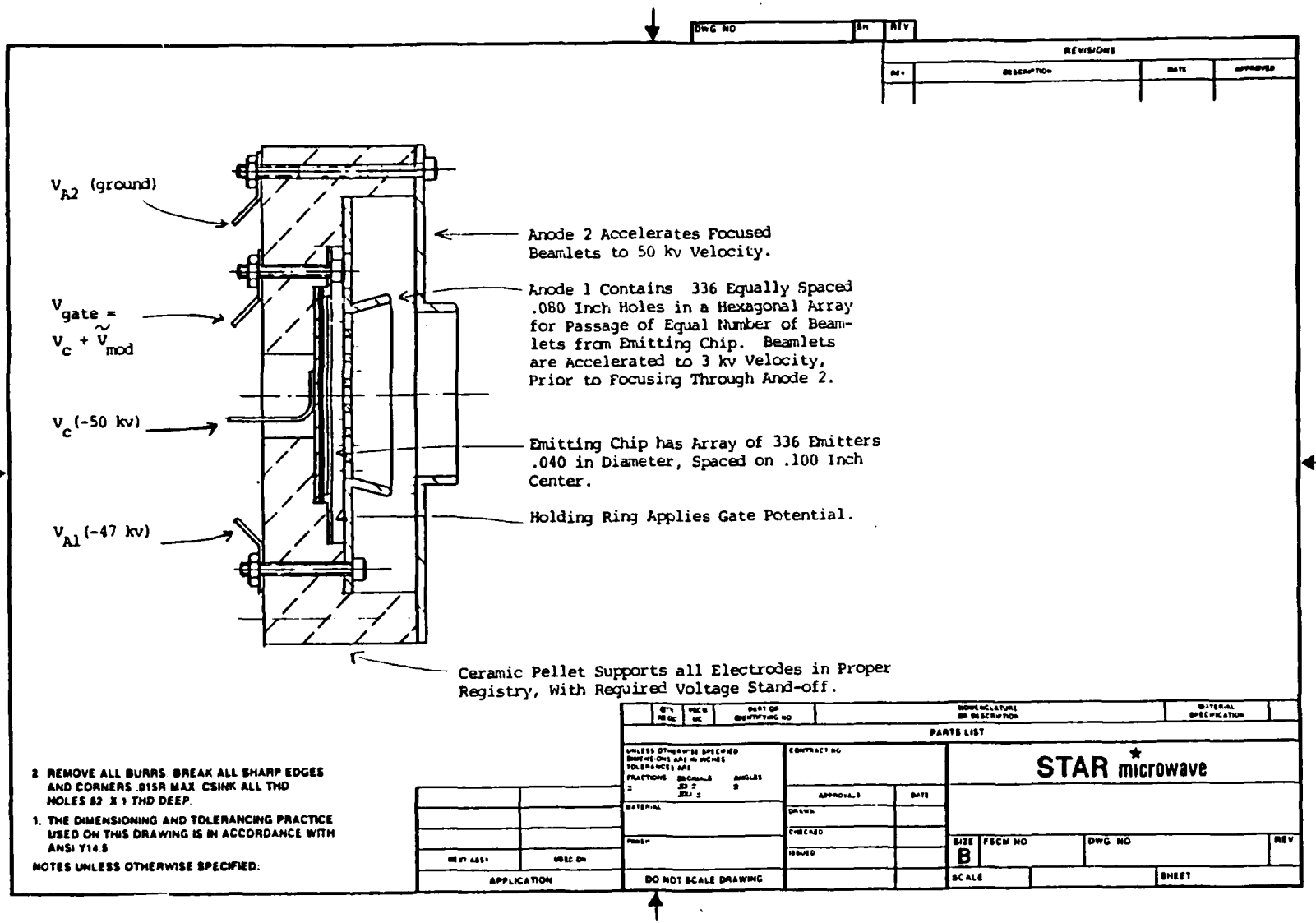

Figure 1: Schematic of Phase 2 10A, 50 kv Modulatable Thin Film Space Gun.

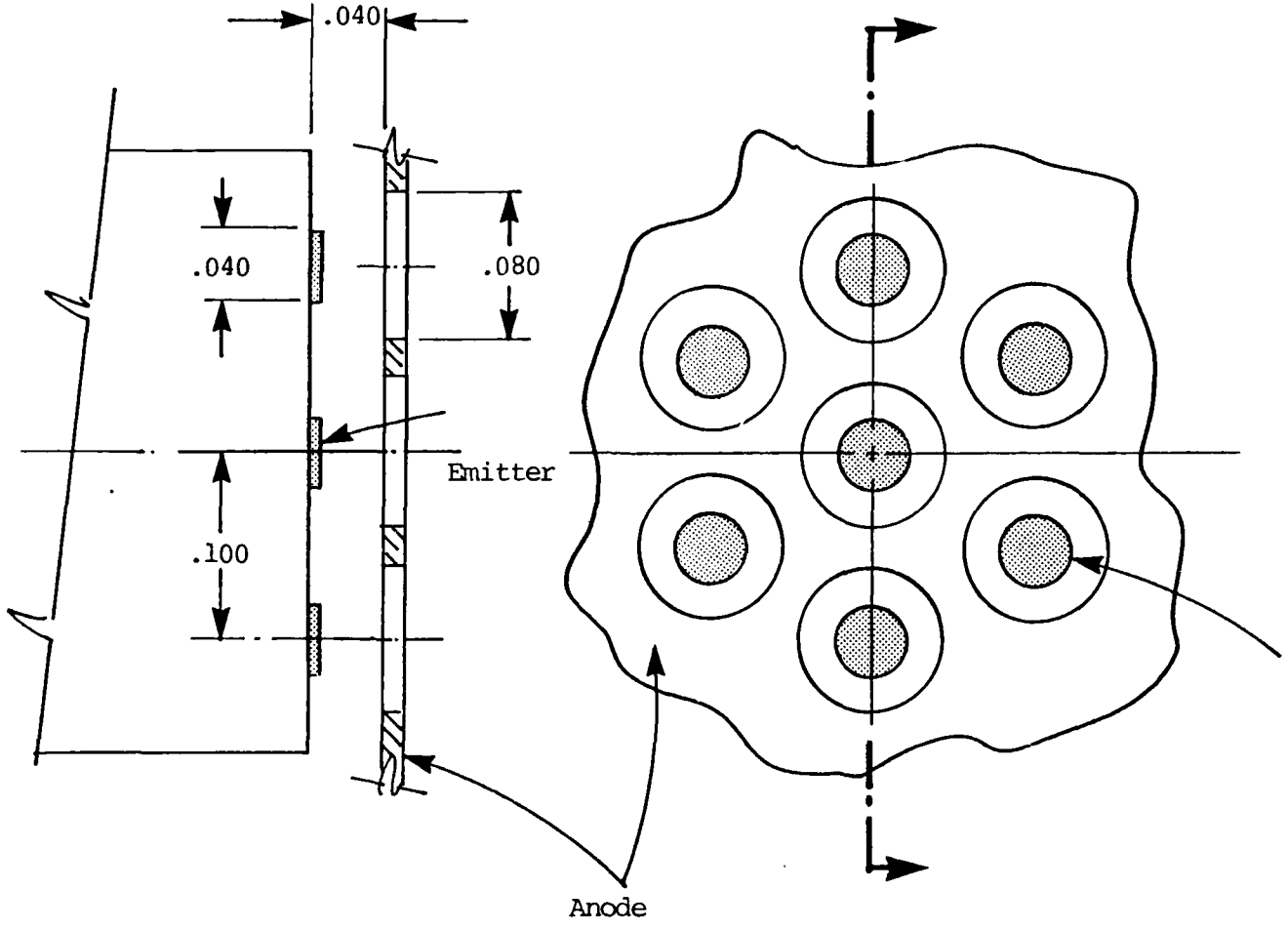

Figure 2: Emitter Hexagonal Array Geometry Proposed For Phase II 2-inch Diameter Chip.

total current from a 2-inch diameter cathode of the proposed geometry, each emitter is required to provide a modest current density of 3.8 amps/cm^2. The total current required of the 1/2-inch by 1/2-inch emitting chip, operating at 3.8 amps/cm^2, is 0.625 amps.

Figure 3 illustrates the operation of the space gun. Emission is through the 3 kv perforated anode with acceleration to 50 kv by the second anode, which is shaped to maintain essentially parallel flow from the throat of the electron gun. Figure 4 is an assembly drawing of the feasibility tester which was built to evaluate the 1/2-inch square standard thin film field emitting chip.

The chip is mounted in a ceramic pellet and is held in place by a retaining ring which is attached to the pellet by two screws. A braze lug and lead are attached to one of the two retaining screws and welded through the ceramic header to provide the gate voltage. The perforated anode is held in registry 40 mils above the emitting chip (20 mils above the retaining ring) and is also bolted to the pellet. The anode voltage is applied to one of its two restraining bolts, again by way of a lead through the high voltage header. The cathode voltage is applied by way of a lead attached to the back of a plate which supports the emitting chip from behind. This lead also passes through the high voltage header. Current is turned off and on by applying relatively low voltage (less than 100 volts) between the gate film and the cathode. The resulting emission is then accelerated through the anode by applying a voltage on the order of 1000 to 3000 volts to the perforated anode.

The feasibility tester does not contain the second accelerating anode (50 kv). Rather, the emitted current is collected on the six-inch long barrel of the space gun tester, which can be conveniently cooled with air or liquid.

The feasibility tester was designed to operate in the same mode as the second phase space gun, i.e., with a grounded anode, negative cathode and with the gate modulated positive with respect to the cathode.

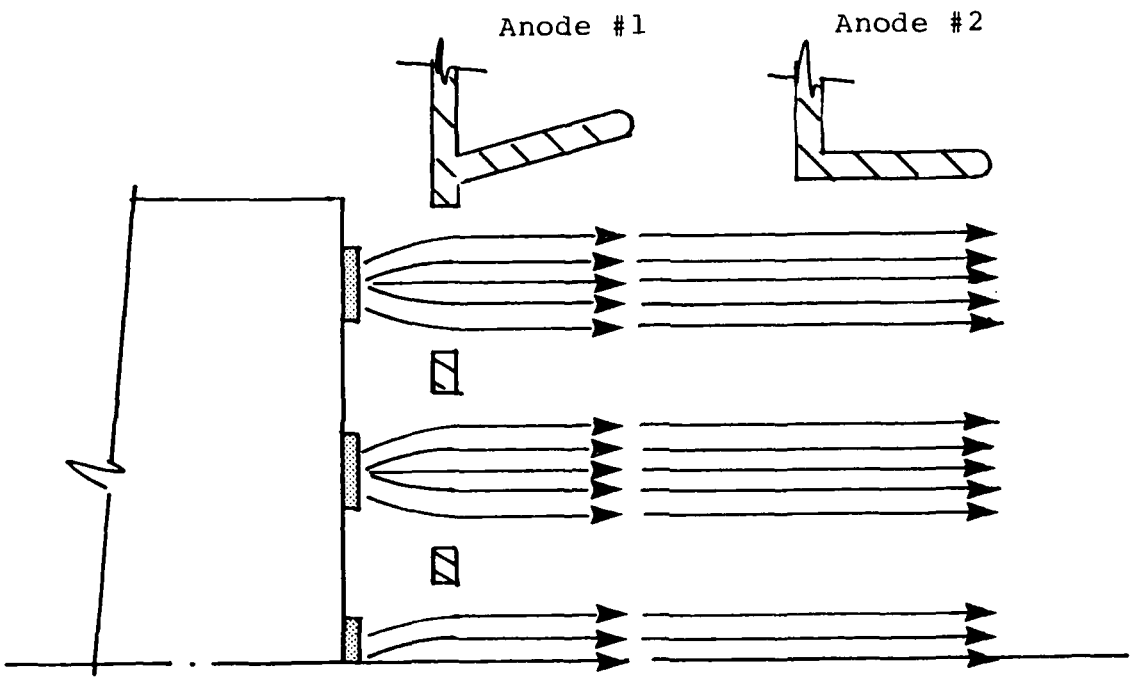

Figure 3: Acceleration of Emission Beamlets Through Perforated Anode.

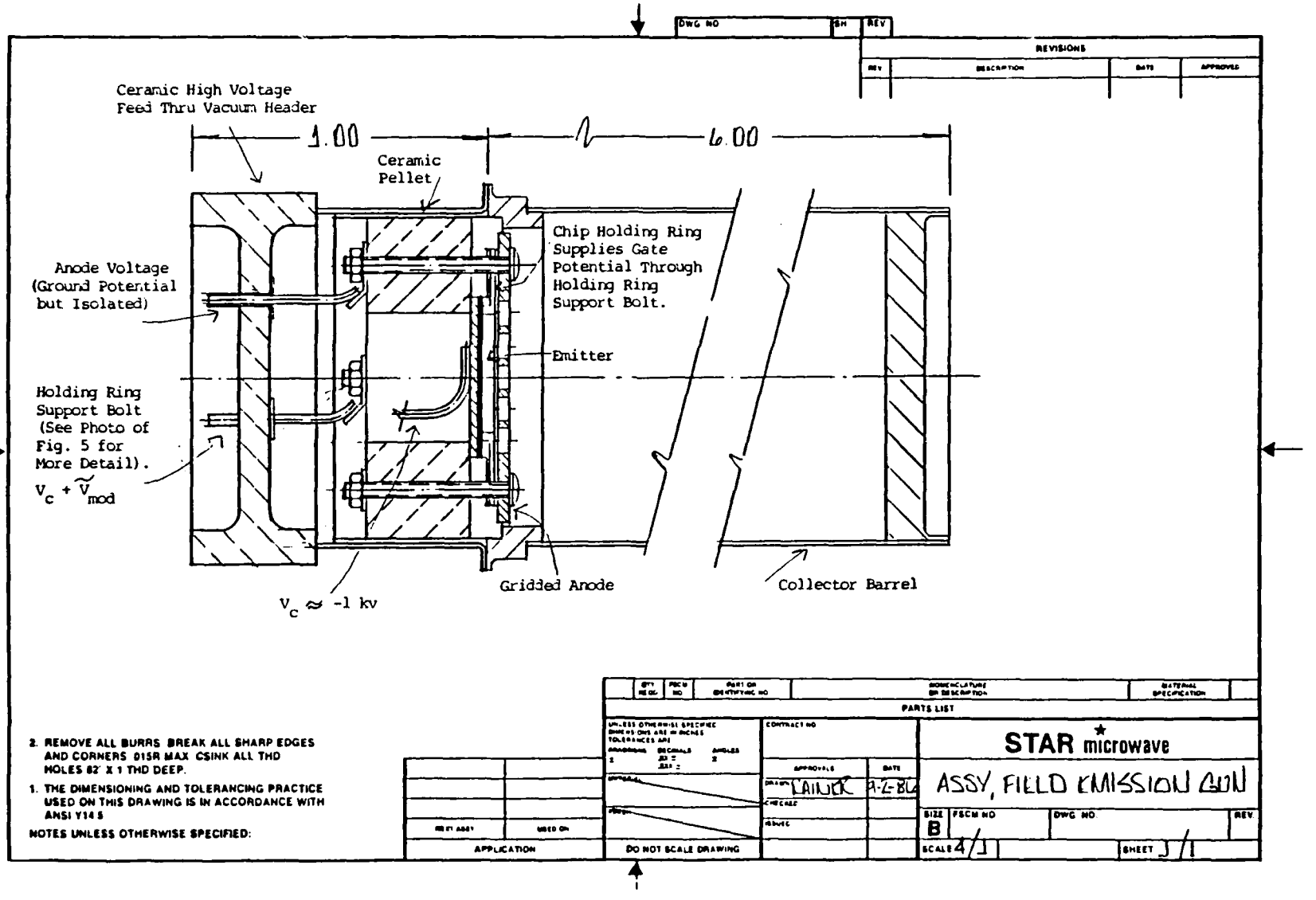

Figure 4: Assembly Drawing of Phase I Space Gun Feasibility Tester.

2.2 Experimental Results

The computer design of the gun optics was completed on schedule, as were the piece parts and subassemblies. The history of the emitting chips best describes the further history of the program. Five chips were fabricated by SRI International.

Chip No. 1 - This chip was subjected to preliminary testing at SRI International. It showed a gate current exceeding 10% of the emitted current, which is unacceptably high. Examination showed that a large fraction of this unaccounted for gate current was caused by unintended or phantom emission. Emitters are deposited in a five by five array as illustrated in Figure 5. Because the four corners provide footpads for the retaining ring, they are masked to prevent the deposit of emitting cones. It was found that the masking was not perfect so that some emitting cones were being produced at the corners. These, of course, emit directly into the footpads of the retaining ring, and appear as gate current. The masking problem was corrected and a second chip was fabricated.

Chip No. 2 - In preliminary tests at SRI, this chip showed improved gate current, but the gate current was felt still to be too high. Some adjustments were made in the chip manufacturing procedure and a third chip was fabricated.

Chip No. 3 - This chip was mounted in the ceramic pellet supplied by STAR Microwave. These original pellets were of machined MACOR glass ceramic. The chip was tested to 1 mA current. It was found to have adequately low gate current and was shipped in its vacuum container to STAR Microwave. The assembly procedure at STAR Microwave was to open the Conflat flange seals on the evacuated chamber and to transfer the pellet to the space gun housing. The leads were threaded through the high voltage header and heliarced to the feed-through. The 6-inch long collector was then to be heliarced in place. This was to be followed by evacuation, 24-hour bake-out and test.

Assembly proceeded with only minor perturbations through the stage where the leads where heliarced to the feed-throughs to

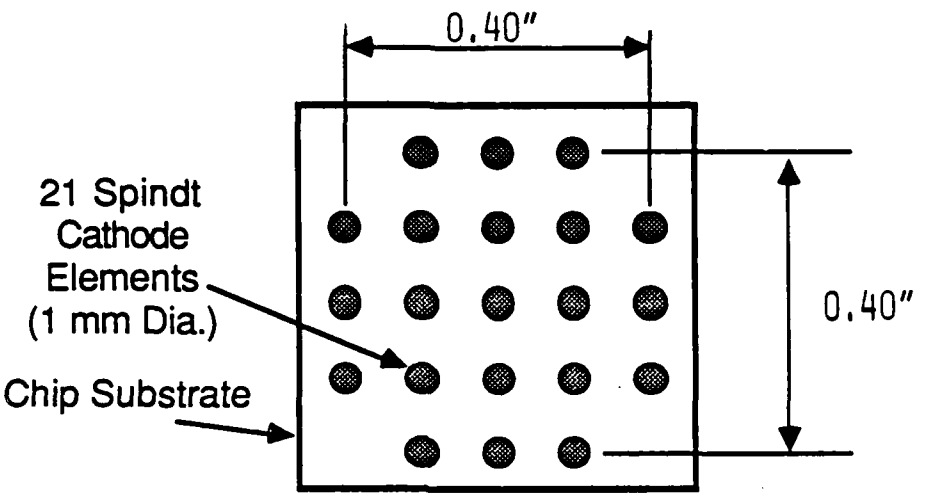

Figure 5. Overall geometry of the Spindt cathode chip with 21 cathode elements.

produce a vacuum-tight assembly. It was observed after heliarcing that the face of the emitting chip was covered with arc marks that, under a microscope, gave the appearance of lightning from emitting hole to emitting hole. A resistance check showed that the emitter was shorted, i.e., the resistance between gate film and cathode had decreased from megaohms to a few hundred ohms.

The pellet and emitting chip assembly was returned to SRI International for analysis. It was concluded there, as it had been at STAR Microwave, that the breakdown was caused by the heliarcing, a welding technique which makes use of RF to initiate and maintain the welding arc. It is believed that enough high power RF coupled to the chip leads to produce the observed breakdown and destruction of the emitting chip.

With this discovery, the space gun was redesigned to eliminate the need for heliarcing the leads through the high voltage header. This was accomplished by using much longer feedthrough tubulations which were closed off by pre-welding at the external ends. The intent was to simply slip the leads from the pellet into the dead ended tubulations, recognizing that the leads would have to make contact in the small diameter tubulations somewhere in the available two inches, so that the electrical connection was assured. A further step in the redesign was to move the heliarc flange which completes the assembly of the six-inch collector to the gun housing to a point well removed from the emitting chip. This change, plus the use of careful grounding of the gun housing was felt to be adequate to make it safe to use the heliarc for this less critical weld without fear of RF damage to the chip.

Analysis of the failed chip at SRI uncovered a second problem. It was found that the chip face was covered by micron size bits of mica. It was surmised that these had to have come from the machined macor pellet, the body of which is made up of glass, interspersed with microscopic mica which makes the material machinable.

Because the presence of these micron size particles would surely cause failure of the emitting chip, it became necessary to

order new pellets made from alumina.

Chip No. 4 - The fabrication of Chip No. 4 was delayed because of a planned refurbishing of the Clean Room facility at SRI International. When Chip No. 4 was fabricated, it was lost prior to preliminary testing as a result of a fracture in the brittle silicon substrate. It seems that this is a fairly common occurrence.

Chip No. 5 - This chip was fabricated, mounted in the new alumina pellet and tested successfully to 1 mA current at SRI International. It was successfully mounted at STAR Microwave in the redesigned space gun. The only area of uncertainty was the discovery that the temporary housing had gone to air at some point between initial testing and its arrival at STAR Microwave.

The space gun was baked out for 24 hours at 450^{o}C, pinched off from the main pump, and the appendage ion pump was activated. A measurement of the resistance between gate film and cathode showed less than 10 megaohms. This, according to SRI International, was less than normal, but usable. In the tests which followed, the chip failed so prematurely and unexpectedly that we were not yet fully instrumented. Hence, the only data from the experiment is the following narrative account put together from notes which were made at the time.

The first step in the testing procedure was to apply voltage between the anode and the pellet with no applied gate voltage. Applying this cathode-anode voltage caused some gassing up of the space gun which was evidenced as increased appendage ion pump current. At about 400 volts there was an arc of undetermined origin. Measurement of the resistance between cathode and gate showed that the megaohms had become a few kilo ohms. It was suggested by C.A. Spindt, in a telephone discussion of the problem with SRI International, that this could possible be cleared by using a capacitor discharge of between 20 and 40 volts between cathode and gate film.

The discharge accomplished the desired result and resistance between cathode and gate film returned to greater than 1 megaohm. After successfully reaching 1 kv between the chip and anode, a

rectified sine wave voltage was applied to the gate film. This produced the characteristic pulses of current, familiar in SRI reports. The current was monitored by passing the leads through current viewing transformers.

It was discovered that the gate current was extraordinarily high, being approximately 40% of the cathode current. This was orders of magnitude higher than the expected leakage current based on gate/cathode resistance. We were not yet equipped to measure anode current. With gate current remaining a steady 40% of cathode current, the latter was increased by increasing the rectified sine wave voltage to about 30 volts, which produced 3 mA of cathode current. At this point, there was another breakdown. Cathode/gate resistance was again measured and found to be less than a thousand ohms. A charged capacitor was again used to clear the short and a cathode/gate resistance in excess of one megaohm was again achieved. The process of gradually increasing the gate voltage was resumed at which time a new phenomena was observed. An increase in gas pressure, as evidenced by ion pump current, resulted in a decrease in both cathode and gate current at a given cathode/gate voltage, i.e., emission was being poisoned.

The chip was allowed to age at a fixed amplitude of rectified sine wave gate voltage until the tester pumped down, at which point emission had recovered. The increase in gate voltage was then resumed, a volt at a time, until at about 35 volts, cathode current had reached 5 mA and gate current 2 mA (still 40%). There was another burst of gas and both cathode and gate current went off scale on the oscilloscope.

Cathode/gate resistance was found to be less than 500 ohms. Attempts to clear the short with a charged capacitor were futile. The gun was opened up and examined under a microscope. One of the corner-most emitters (see Figure 5) was largely destroyed (see Figure 6). The remaining 20 emitters appeared visually to be relatively unaffected. The reason for the breakdown and destruction is not known.

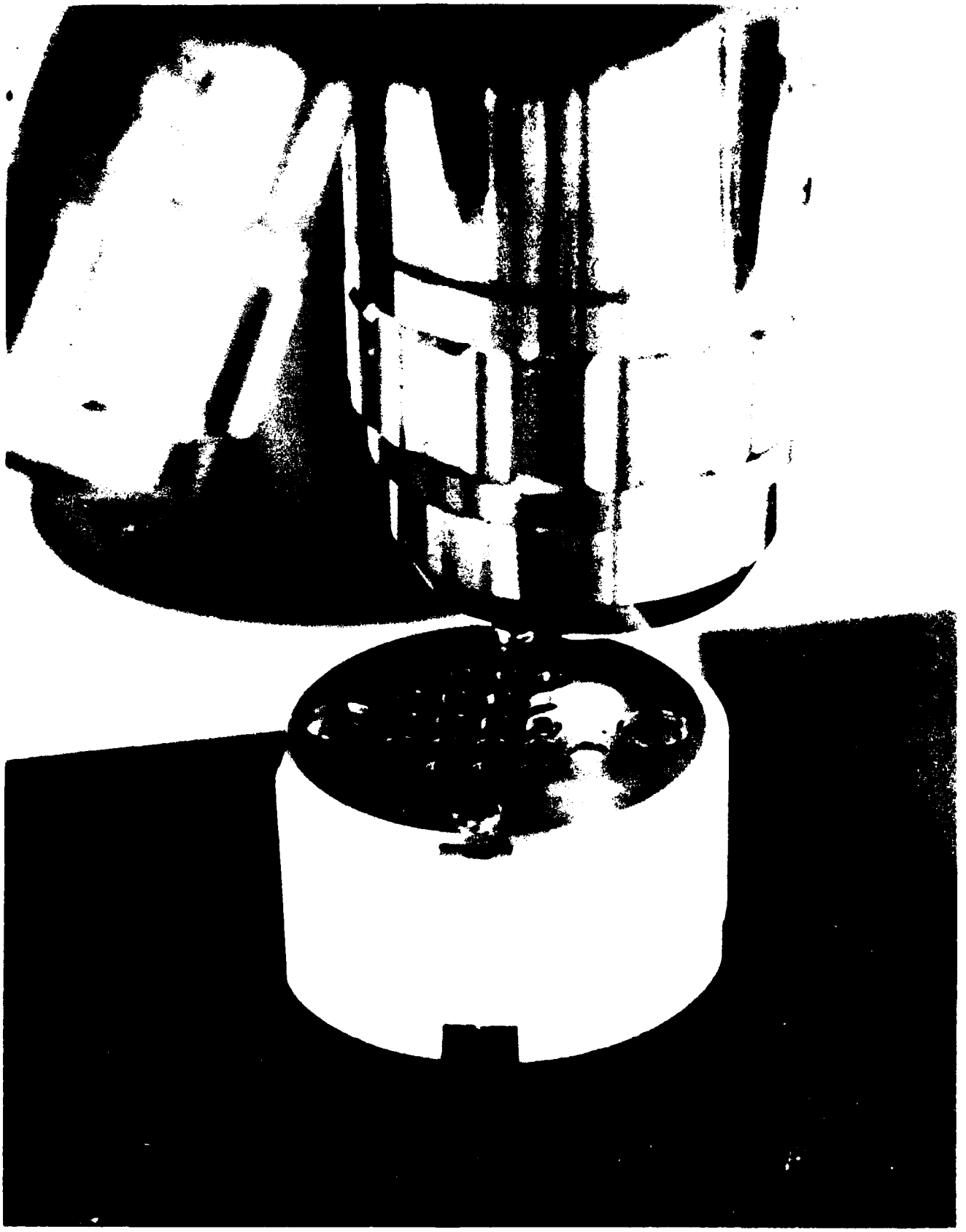

Figure 6: Pellet Assembly Being Examined Under Microscope. Emitter Under Lighted Anode Hole Experienced Massive Failure of Figure 7.

Figure 7: View through Microscope of Emitter Failure. Magnification is Approximately 1400 to 1. Emitter Holes (Array of 12,500 Emitters) are Clearly Visible.

Permission has been granted from the publisher to reproduce the following article, "Physical Properties of Thin Film Field Emission Cathodes" which is to be used as an appendix to this report on Contract F19628-85-C-0088.

APPENDIX I

THEORY OF SPINDT THIN FILM FIELD EMITTER

The following article describes the theory of the field emitter which was investigated for use as a source of amperes of modulated current. The article is reprinted from the Journal of Applied Physics, Vol. 47, No. 12, Dec. 1976. The authors are C.A. Spindt, I. Brodie, L. Humphrey and and E.R. Westerberg.

Physical properties of thin-film field emission cathodes with molybdenum cones

C. A. Spindt, I. Brodie, L. Humphrey, and E. R. Westerberg

Stanford Research Institute, Menlo Park, California 94025
(Received 18 March 1976; in final form 15 July 1976)

Field emission cathodes fabricated using thin-film techniques and electron beam microlithography are described, together with effects obtained by varying the fabrication parameters. The emission originates from the tip of molybdenum cones that are about 1.5 μm tall with a tip radius around 500 Å. Such cathodes have been produced in closely packed arrays containing 100 and 5000 cones as well as singly. Maximum currents in the range 50–150 μA per cone can be drawn with applied voltages in the range 100–300 V when operated in conventional ion-pumped vacua at pressures of 10^{-9} Torr or less. In the arrays, current densities (averaged over the array) of above 10 A/cm^2 have been demonstrated. Life tests with the 100-cone arrays drawing 2 mA total emission (or 3 A/cm^2) have proceeded in excess of 7000 h with about a 10% drop in emission current. Studies are presented of the emission characteristics and current fluctuation phenomena. It is tentatively concluded that the emission arises from only one or a few atomic sites on the cone tips.

PACS numbers: 79.70.+q, 29.25.Bx, 52.80.Vp

I. INTRODUCTION

Several years ago Spindt and his co-workers at SRI[1,2] developed methods for fabricating arrays of minute cones for use as field emission cathodes by evolving new techniques in thin-film technology and electron beam microlithography. Since that time the technology of fabrication has been advanced, taking advantage of improvements in silicon thin-film technology instigated by the growing needs of the semiconductor industry. The technology now allows the cathodes to be made in arrays of up to 5000 cathodes at packing densities up to 6.4×10^5/cm^2.

Apart from the precision with which individual cones may be positioned and the ability to pack large numbers of identical cones into small areas, a major advantage offered by these cathodes is the very low voltages at which they operate. These voltages range from 100 to 300 V for useful emission, compared with values ranging from 1000 to 30 000 V for conventional etched wire emitters. This low-voltage operation is achieved by placing the accelerating electrode close to the tip and making the radius of the tip very small. The low voltage of operation of these cathodes makes them less vulnerable to damage by ionization of the ambient gas.[3] Hence, the low voltage allows the cathodes to operate continuously with very stable emission properties and long life, at pressures higher than those necessary for conventional field emitters, and without resorting to strategems of intermittent or continuous heating. Furthermore, the arrays are capable of operating at effective current densities (averaged over the area of the array) of greater than 10 A/cm^2 continuously, far higher than can be obtained with thermionic cathodes with a reasonable life expectancy.[4]

Molybdenum is a particularly good material to use for the sharp pointed cones, from which the electrons are emitted. A high degree of reproducibility has been achieved with this material, even though the cathodes cannot be heated to the temperatures necessary to completely remove absorbed and dissolved gases from the region of the emitting area. Molybdenum is not considered to be necessarily the ideal material for the cone, and studies are now being made using materials with lower work functions to further decrease the operating voltages. However, molybdenum has properties that are very useful in fabricating cones and a large amount of the data has been accumulated on this material. The purpose of this paper is to describe the manufacture and properties of this type of thin-film field emission cathode and compare its performance with conventional etched molybdenum cathodes.

II. DESCRIPTION OF THE TFFEC AND ITS METHOD OF FABRICATION

The thin-film field emission cathode (TFFEC) con-

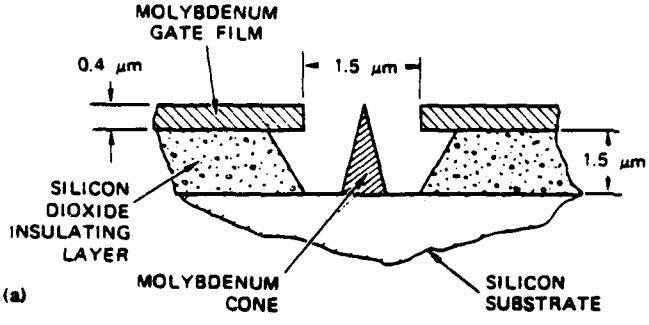

FIG. 1. Schematic diagram and scanning electron micrograph of a thin-film field emission cathode (TFFEC).

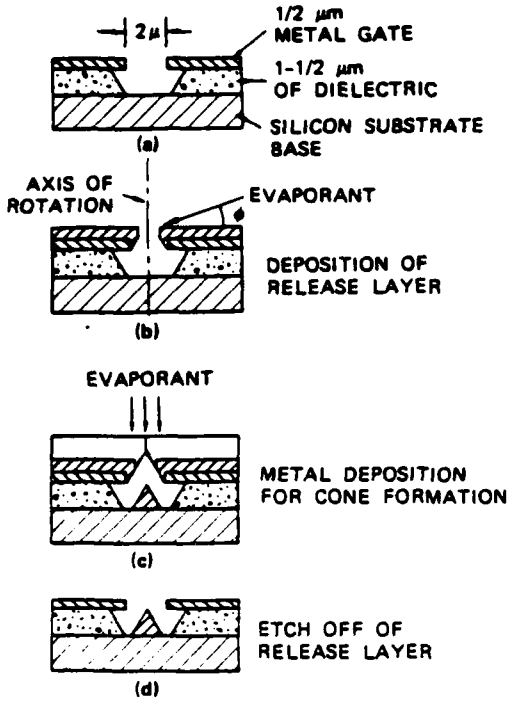

FIG. 2. Thin-film field emission cathode fabrication.

sists basically of a conductor/insulator/conductor sandwich (Fig. 1). The top conductor or gate film has holes of from 1.0 to 3 μm in diameter in it, through which a cavity can be etched in the insulator. This cavity undercuts the gate and uncovers the substrate conductor. A metal cone whose base is attached to the substrate and whose tip is close to the plane of the gate film is then formed in the cavity.

Heavily doped silicon is preferred as the substrate, since silicon dioxide can be grown on its surface to thickness of around 1 μm with excellent adherence, no porosity, and high-field breakdown strength. A film of molybdenum (about 0.4 μm thick) is vacuum deposited on the silicon dioxide to provide the gate electrode. The cone height, tip radius, and gate aperture are variables of the fabrication technique that offer some control over the current-voltage characteristic, as discussed in Sec. III D,

The present method of fabrication is as follows:

(a) Obtain standard 5-cm-diam silicon wafers, 0.75 mm thick of highly conducting (0.01 Ω/cm) silicon, as are used for semiconductor fabrication.

(b) Oxidize the wafers to the desired thickness—usually about 1.5 μm—using standard oxidation techniques.[5]

(c) Cut wafers into squares of a size suitable for handling by scribing and breaking.

(d) Coat the oxide with a uniform layer (0.4 μm thick) of molybdenum. Electron beam evaporation is more convenient for this purpose than sputtering.

(e) Coat the squares on the molybdenum side with an electron-sensitive resist, PMM (poly-methyl-methacrylate), to a thickness of about 1 μm, using standard spinning methods.[6]

(f) Expose the resist-coated surface in vacuum to a pattern of electron beams focused to form an array of spots in the desired configuration. The electron projection techniques were devised by Westerberg, and the details of these techniques are given elsewhere.[7] The exposed spots are usually about 1 μm in diameter. Square arrays on 25.4- and 12.7-μm centers have been made.

(g) Remove the PMM that has been exposed to electrons, by dissolving these areas in isopropyl alcohol, exposing the underlying molybdenum. Then, selectively etch the molybdenum through to the silicon dioxide layer.

(h) Remove the remaining PMM. Then, etch the silicon dioxide down to the silicon base with hydrofluoric acid solution. At this point, the structure takes the form illustrated in Fig. 2(a). The molybdenum layer is undercut by removal of silicon dioxide, since the acid does not attack molybdenum.

(i) Mount the substrate in a vacuum deposition system and rotate the substrate about an axis perpendicular to its surface. A parting layer of aluminum is deposited at grazing incidence. In this way the size of the holes can be decreased to any desired diameter [Fig. 2(b)].

(j) Deposit molybdenum through the partially closed holes by electron beam evaporation from a small source at normal incidence. The size of the hole continues to decrease because of condensation of molybdenum on its

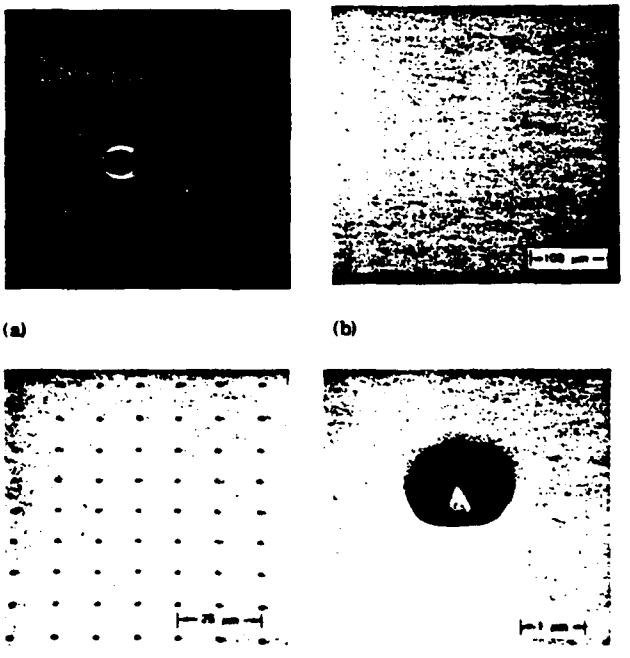

FIG. 3. An array of 5000 thin-film field emission cathodes on 0.0005-in. centers. (a) Cathode chip mounted on a ceramic holder. (b) Portion of the 5000-tip array magnified. (c) High magnification of part of the array. (d) Ultrahigh magnification of a tip in the array.

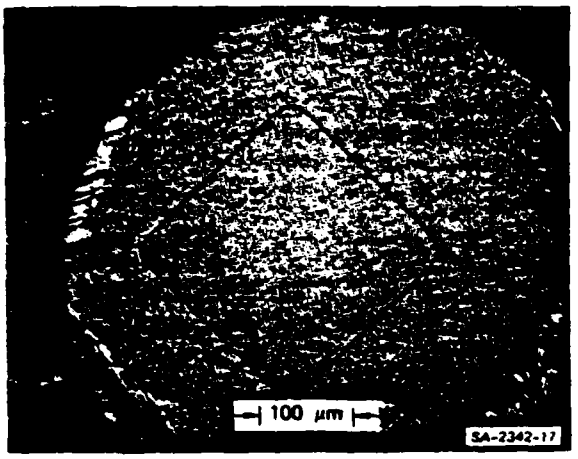

FIG. 4. Micrograph of cathode array showing the results of sandwich breakdown between two of the cones and the gate film.

periphery. A cone grows inside the cavity as the molybdenum vapor condenses on a smaller area, limited by the decreasing size of the aperture. The point is formed as the aperture closes. Considerable control of the cone height, angle, and tip radius is obtained by choice of the starting aperture size, the thickness of oxide layer, and the distance of the evaporation source from the substrate.

(k) Dissolve the parting layer of aluminum, releasing the molybdenum film deposited during the cone formation step. After a thorough cleaning, the cathode is ready for mounting in a vacuum tube.

Using these procedures, cathodes with 1, 100, and 5000 emitting cones have been grown. The 100-cone array was arranged in a 10×10 matrix with 25.4 μm spacing, the total cathode area covering a square that is 0.25 mm on each side. The 5000-cone array was arranged in a circular area 1.0 mm in diameter, with the emitting cones placed in a rectangular matrix with 12.7 μm spacing. Figure 3 shows a 5000-cone array at various magnifications. The data shown in Figs. 3(c) and 3(d) were obtained with a scanning electron microscope.

The cathodes were mounted on a ceramic header and spaced at a suitable distance from a metal collector electrode. Tests are made in ion-pumped systems at ambient pressures of 10^{-9} Torr or less. Stringent high-vacuum procedures (including a 350—450 °C bakeout) were necessary to avoid disruption of the cathode early in life. This disruption appears to be caused by a local gas discharge forming between the tips and the gate electrode. After such disruption the cathode takes the appearance shown in Fig. 4.

Note that single elements can be disrupted without destroying the whole array. Also, the site where the discharge occurred usually remains open-circuited between the base and the gate so that the device is still operable. Outgassing of the active components of the tube, including the cathode itself, is the main source of gas for this discharge. This effect can be essentially eliminated by bombarding all the active parts of the tube (including the cathode) with electrons from a separate tungsten thermionic filament, appropriately disposed in the tube.

An important difference between the TFFEC and the conventional etched wire field emitter is that TFFEC cannot be heated to temperatures above 700 °C, due to distortion caused by the stresses set up by the different thermal expansions of the component layers. Thus, the adsorbed gases on the surface of the tip and sources for their replenishment by surface or solid diffusion are never completely removed. Furthermore, the growth of a single crystal at the tip, with the usual field/heat emission enhancement effects due to buildup at the crystal boundaries, is not evident.

Field emission micrographs from a single TFFEC point were made, and one or a few lobes were observed without regular structure. Twinkling and movement of the lobes were observed.

III. EMISSION PROPERTIES

A. Theoretical background

The generally accepted Fowler-Nordheim theory[3] for a clean metal surface relates the field emission current density, J, to the electric field at the surface, E, in volts/cm and the work function ϕ in electron volts by the equation

$$J=\frac{AE^2}{\phi t^2(y)}\exp\left(-B\frac{\phi^{3/2}}{E}v(y)\right)\frac{\text{A}}{\text{cm}^2}\,, \tag{1}$$

where

$$A=1.54\times10^{-6},$$

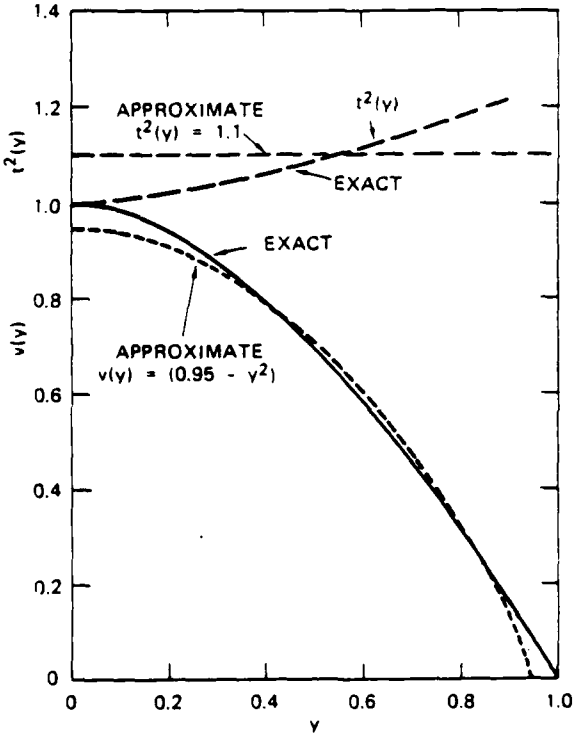

FIG. 5. Comparison of approximate forms with exact solutions for the Fowler-Nordheim field emission functions $v(y)$ and $t^2(y)$.

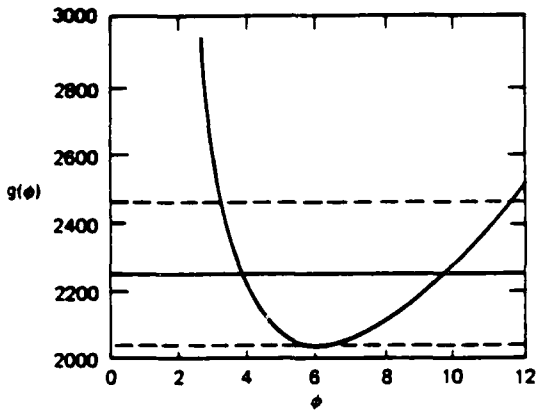

FIG. 6. $g(\phi)$ as a function of ϕ.

$$B = 6.87 \times 10^7,$$

$$y = 3.79 \times 10^{-4} E^{1/2}/\phi .$$

y is the Schottky lowering of the work-function barrier.

The functions $v(y)$ and $t(y)$ have been computed[9] and, as can be seen from Fig. 5, we can use as a close approximation over the operating range of most cathodes the following values:

$$t^2(y) = 1.1 \quad \text{and} \quad v(y) = 0.95 - y^2. \tag{3}$$

Typically, the field emission current I is measured as a function of the applied voltage V and we can substitute $J = I/\alpha$ and $E = \beta V$ in Eq. (1), where α is the emitting area and β is the local field conversion factor at the emitting surface. Combining these relationships gives

$$I = aV^2 \exp(-b/V), \tag{4}$$

where

$$a = \frac{\alpha A \beta^2}{1.1\phi} \exp\left(\frac{B(1.44 \times 10^{-7})}{\phi^{1/2}}\right), \tag{5}$$

$$b = 0.95 B \phi^{3/2}/\beta. \tag{6}$$

By differentiating Eq. (4) we obtain

$$\frac{dI}{dV} = \frac{I}{V}\left(2 + \frac{b}{V}\right). \tag{7}$$

Thus, by measuring I, V, and dI/dV at any given point on the current-voltage characteristic we may obtain the value of b at a specific current I from Eq. (7). Substitution of b/V in Eq. (4) gives a.

Since we have three unknown constants to determine in a given field emission situation—namely, α, β, and ϕ—it is impossible to separate them with a knowledge of a and b only. An independent method must be found of measuring one of them or finding some other relationship between them.

Following Van Oostrom[10] and Charbonnier and Martin,[11] we note that

$$ab^2 = \frac{(0.95)^2}{1.1} \alpha A B^2 \phi^2 \exp\left(\frac{B(1.44 \times 10^{-7})}{\phi^{1/2}}\right),$$

$$ab^2 = \alpha(5.96 \times 10^9)\phi^2 \exp(9.89/\phi^{1/2}). \tag{8}$$

The function $g(\phi) = \phi^2 \exp(9.89/\phi^{1/2})$ is plotted in Fig. 6 over the range $\phi = 1$ to $\phi = 12$. This shows that if a fixed value of $g(\phi) = 2250$ is chosen, then the error will not be greater than $\pm 10\%$ over the range $\phi = 3.4$ to $\phi = 11.6$. Fortunately, this covers the work-function range of many practical field emitters. Using the above value for $g(\phi)$ enables us to estimate the emitting area α to $\pm 10\%$ from the relation

$$\alpha = ab^2/(1.34 \times 10^{13}) \quad \text{cm}^2. \tag{9}$$

Combining Eqs. (4) and (9) we obtain

$$\frac{\alpha}{I} = \frac{(b^2/V)\exp(b/V)}{1.34 \times 10^{13}}. \tag{10}$$

This relationship is plotted in Fig. 7 for values of b/V in the range 5—15. This covers the practical range for field emission. Figure 7 shows clearly that to estimate α within a factor of 3, b/V must be obtained with a precision of better than $\pm 10\%$.

Equation (7) gives

$$\frac{b}{V} = \frac{V}{I}\frac{dI}{dV} - 2 \tag{11}$$

so that the individual measurement of V, I, and dI/dV must be precise to about 1% for this method to have an error even approaching that of Eq. (9) for the emission area. In practice dI/dV is difficult to measure with the required precision.

As can be seen from this analysis, the order of magnitude of the apparent emitting area α can be obtained by the measurement of I, V, and dI/dV, provided the cathode is aged to the point where good Fowler-Nordheim plots are obtained.

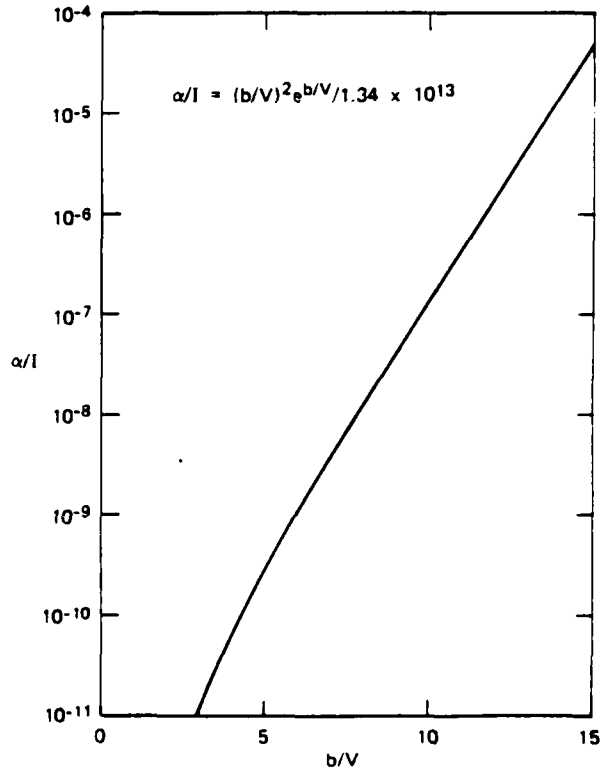

FIG. 7. α/I as a function of b/V.

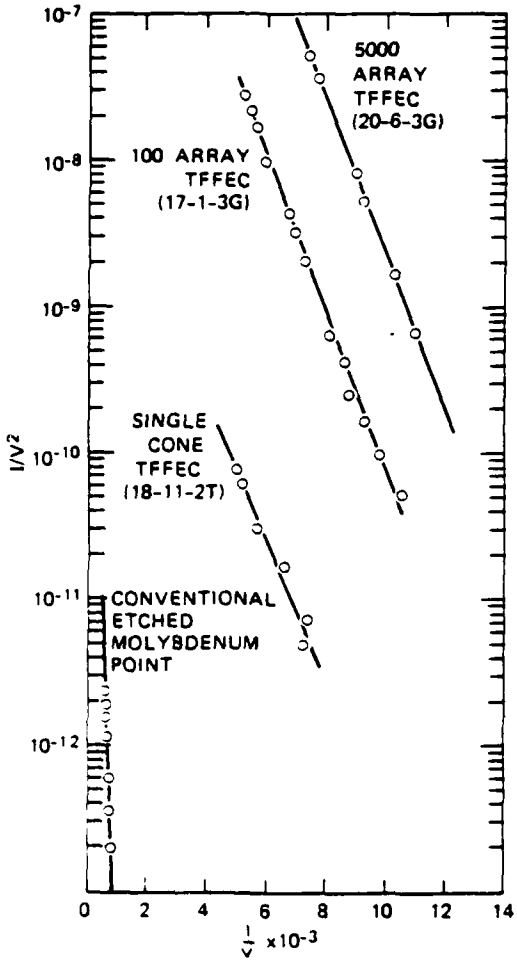

FIG. 8. Fowler-Nordheim plots for representative cathodes.

B. Current-voltage characteristics

In Fig. 8 Fowler-Nordheim plots for different varieties of cathodes—namely, single-cone TFFEC's, arrays of 100 TFFEC's, and arrays of 5000 TFFEC's—are compared with an etched molybdenum wire. The etched wire was not heat treated, so the condition of its tip was similar to that of the TFFEC cones. Etched wire emitters show considerable variability in their emission performance from one sample to another. Although they all evinced straight-line Fowler-Nordheim plots, the voltage to draw 1 μA of emission varied from 1000 to 2500 V.

As will be seen, reasonable straight lines are obtained for the TFFEC's and, in the samples chosen, are nearly parallel to each other. The displacement is approximately equal in ratio to the number of emitting points. Differences among the cathodes are attributed mainly to different dimensions in the samples of cone heights, gate hole diameters, and tip radii.

An important conclusion from these results, verified by scanning electron microscope studies, is that the individual cones in any given array must be almost identical, with a very small spread in the field conversion factor β among them. We note from Dyke and Dolan's tables[12] that a deviation of E $(=\beta V)$ of only 20% from the average would increase or decrease the emission of an individual cone by a factor of more than 10 (assuming a work function of about 4.5 eV and fields of about 5×10^7 V/cm).

The maximum current that can be drawn from a single TFFEC tip is usually in the range 50—150 μA for a well-aged tube. If the current exceeds this value the cone completely disrupts in a manner analogous to the disruption of field emitting whiskers in vacuum breakdown.[13] Currents up to 5 mA (corresponding to an effective current density of 8 A/cm^2) have been drawn from the 100-cone arrays on 25.4-μm centers and, under pulse conditions, currents of up to 100 mA (corresponding to a current density of 12 A/cm^2) have been drawn from 5000-cone arrays on 12.7-μm centers. In the latter case the main difficulty in reaching an anticipated 50 μA $\times$ 5000 = 250 mA (or 30 A/cm^2) current has been associated with the anode of the tube, which was not designed to dissipate the powers involved.

C. Estimation of the emitting area

We attempted to measure the emitting area of the cones using the method described in Sec. III A. Average values of dI/dV were obtained by precise measurements of the change of I with V around the point under consideration and by using the lock-in amplifier technique. Results for the above cathodes are shown in Table I. Apparent emitting areas of the TFFEC's are of the order of 1.2×10^{-15} cm^2/cone compared to values of 160×10^{-15} and 71×10^{-15} cm^2 for two etched points.

If these results are taken at their face value, it would

TABLE I. Estimates of apparent emitting areas by the Fowler-Nordheim method.

Cathode	Number of tips (n)	V	I	$\frac{dI}{dV}$	$\frac{b}{V}$	$\frac{\alpha}{I}$	Total apparent emitting (α)	Average apparent emitting area per tip (α/n)
18-11-2T	1	139	1.92×10^{-7}	1.3×10^{-8}	7.41	7×10^{-9}	1.3×10^{-15}	1.3×10^{-15}
17-1-3G	100	136	3.0×10^{-6}	2.0×10^{-6}	7.07	4.3×10^{-9}	1.3×10^{-13}	1.3×10^{-15}
20-6-3G	5000	137	1.0×10^{-3}	7.1×10^{-6}	7.72	1.0×10^{-8}	1.0×10^{-11}	2.0×10^{-15}
Etched wire No. 1	1	2244	1.0×10^{-6}	5.4×10^{-9}	10.1	1.6×10^{-7}	1.6×10^{-13}	160×10^{-15}
Etched wire No. 2	1	1415	1.19×10^{-6}	9.5×10^{-9}	9.3	6×10^{-8}	7.1×10^{-14}	71×10^{-15}

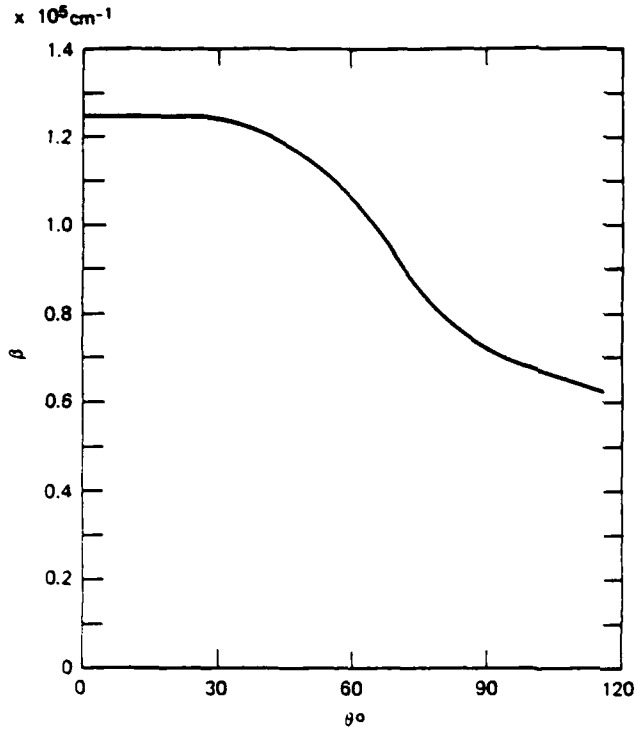

FIG. 9. Field conversion factor β as a function of the polar angle θ for the cone tip of a TFFEC.

appear that only a few atomic sites at the very tip of the cones are contributing to the emission. The observation is well known[10,14] that field emitters that have not been treated by the usual field/heat methods to clean and "build up" the tips give anomalously low areas. This phenomenon has been attributed to the fact that the surface remains contaminated with adsorbed gas. Experiments in which gas is introduced after the tip has been cleaned appears to corroborate this conclusion. Gomer (Ref. 16, p. 50) has shown that the empirical assumption of a linear variation of work function with electric field, as might be expected from an adsorbed monolayer or other surface and band structure effects, leads to an apparent reduction in emission area by a factor

$$f = \exp(3\gamma\beta b/2\phi_0) \tag{12}$$

by assuming $\phi = \phi_0 + \gamma E$, where ϕ_0 is the work function at zero field. The assumption of a linear variation of work function with field is directly analogous to the commonly assumed linear variation of work function with temperature in thermionic emission that is used to interpret the thermionic constants.[15] Gomer's derivation also shows clearly that if f were smaller than 10^{-3} this variation would begin to cause noticeable deviations from the Fowler-Nordheim law.

Due to the perfection with which the cathodes are made, we could measure the dimensions of the critical parameters that govern the field at the cone tip with considerable precision using the scanning electron microscope (SEM) down to the resolution of the instrument used, which was about 100 Å.

A representative set of dimensions (see Fig. 10) was as follows: thickness of gate electrode, $t = 0.4$ μm; diameter of hole in gate electrode: $D = 1.3$ μm; thickness of insulating layer, $d = 1.4$ μm; cone height, $h = 1.4$ μm; cone base diameter, $b = 1.0$ μm; tip radius, $r = 0.05$ μm. These dimensions were used to compute the electric field around the tip. This computation was made using a CDC 6400 digital computer and the relaxation methods to solve Laplace's equation in the interelectrode region. By using successively smaller mesh sizes, the equipotentials could be obtained to any desired degree of accuracy.

In Fig. 9 the calculated field conversion factor β is plotted as a function of the polar angle θ measured from the center of curvature of the tip. It is seen that the field is essentially constant for 30° and then begins slowly dropping off. The value of β at the center, namely, $\beta_0 = 1.25 \times 10^5$ cm^{-1}, compares with a value for an isolated sphere radius 0.05 μm with a concentric spherical anode of radius 0.65 μm of $\beta_0 = 2.17 \times 10^5$ cm^{-1}. This reduction from the isolated sphere case of a factor of 1.7 is reasonable, in view of the presence of the shank and the fact that plane-parallel electrodes are used. This compares with a reduction factor of 5 mentioned by Gomer[16] for a conventional free-standing tip with the anode essentially at infinity.

The effective emitting area can be roughly defined by the angle where the field has dropped off by 10% and the current density has been reduced by a factor of 5. Using this criterion the emitting area would be defined by a spherical cap radius of 0.05 μm and a half-angle of 53° or 6.3×10^{-11} cm^2. This area is more than 10^4 times greater than that estimated from the current-voltage characteristics. The field at the tip with 139 V applied would be 1.74×10^7 V/cm^2. To obtain 1.92×10^7 A from the above area, corresponding to a current density of 3×10^5 A/cm^2, would require the work function to be about 2.6 eV. Polycrystalline molybdenum has a work function of 4.35 eV,[15] and the types of contamination encountered in normal vacuum systems is likely to increase the work function. For example, a monolayer of oxygen adsorbed on molybdenum increases the work function by 1.5 eV, although nitrogen decreases the work function by 0.7 eV. However, it seems unlikely that the tip could have a work function as low as 2.6 eV, since this would require the adsorption of a highly electropositive material such as barium. If we assume that the area given by the current-voltage characteristic is correct, then the current density at 139 V would be 1.7×10^8 A/cm^2. Using this current density and the work function for clean molybdenum, 4.35 eV, we estimate from Dyke and Dolan's tabulation of the Fowler-Nordheim equation that the electric field at the surface would be 8×10^7 V/cm. This high field value would argue that the emitting atoms form a protuberance on the tip of the cone with a field magnification factor of $8/1.74 = 4.6$. This magnification factor is close to that of a hemisphere on a plane which is 3.

Thus it is seen that the results are consistent with the hypothesis that the emission area is close to that given by the F/N method of Sec. III A and that the high field over a small area is caused by a protuberance on the tip. The results are inconsistent with the hypothesis that the tip is smooth and that the area reduction factor

TABLE II. Effect of changes of cathode dimensions in the 100-cone array. (Dimensions in μm.)

Cathode	x	r	D	V for 100 μA
17-13-15	0	0.050	1.3	120
17-18-1 E	0	0.050	1.7	180
17-18-1 I	0	0.060	1.9	225
17-13-15-F	+1.05	0.050	1.3	50
17-13-15 E	0	0.050	1.3	120
17-13-15 G	+0.14	0.050	1.3	80
17-13-20 G	−0.28	0.050	1.3	200
17-13-15 B	+0.84	0.065	1.9	100
17-18-1 I	0	0.060	1.9	225
17-18-1 H	+0.28	0.060	1.9	190
17-18-1 D	0	0.100	1.7	180
17-18-1 E	0	0.050	1.7	180
17-13-16 G	−0.075	0.050	1.6	125
17-13-16 H	−0.075	0.130	1.6	120

is explained by a linear work-function dependency on the field. This is because a smooth surface would require that the work function of the surface be 2.6 eV which is unreasonably low, and an area reduction factor of over 10^4 would require substantial deviation from the Fowler-Nordheim law which is not observed.

D. Effects of cathode dimensions on performance

The 100 emitter arrays were tested to ascertain the effect of change of geometry on the emission. The geometry was measured using the SEM and the emission was characterized by determining the voltage required to obtain 100 μA of emission current after the tube had stabilized. The SEM was also used to determine whether or not any tips were lost during processing. Some results grouped to illustrate the effects of three of the variables are given in Table II. In this table x is the distance of the tip above (+) or below (−) the lower plane of the gate electrode, and the other parameters, r and D, are as illustrated in Fig. 10. From these results, we see that the tip emission is strongly dependent on the diameter of the hole in the gate electrode [Fig. 11(a)] and on the position of the tip with respect to the lower plane of the gate electrode [Fig. 11(b)]. If the tip is made to protrude through the hole, the cathode can be made to operate at as low as 50 V to obtain an emission of 100 μA. One surprising aspect is that variation in the tip radius appears to have a second-order effect on the emission over the range 500—1500 Å.

The results indicate that protruding cones, with D as small as possible, should be used. However, as a practical limit, it has proved difficult to form cones that protrude through the hole in the gate electrode with values of D less than 1 μm without reducing the oxide thickness.

E. Maximum emission per cone

The current that can be drawn from an individual cone is limited by the initiation of a vacuum arc, which completely disrupts the top of the cone. Figure 12 shows the effect of a particularly violent disruption of a single cone in a 5000-cone array TFFEC. It will be noted that despite the splatter of material only one cone was affected and no chain of disruption events was set in

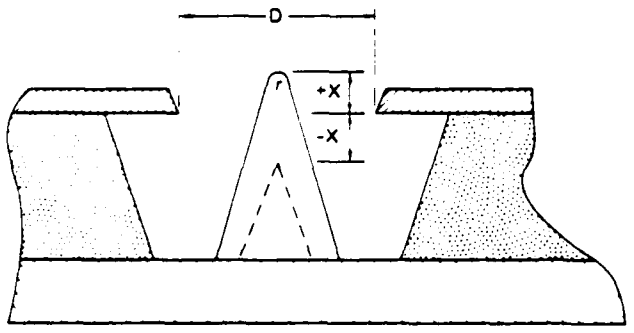

FIG. 10. Parameter definition.

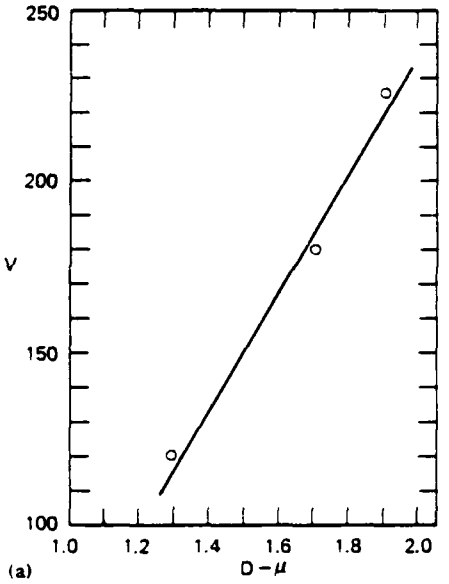

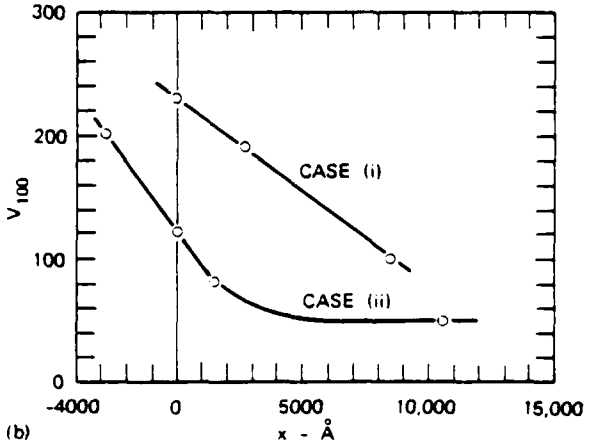

FIG. 11. (a) Voltage for 100 μA as a function of D; $r = 500$ Å, $x = 0$. (b) Voltage for 100 μA as a function of x. Case (i) $r = 600$ Å, $D = 1.9$ μm; case (ii) $r = 500$ Å, $D = 1.3$ μm.

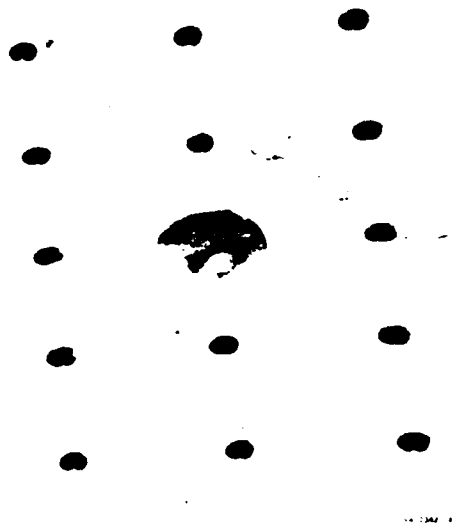

FIG. 12. Disruption of a single cone in a 5000-array TFFEC.

motion. The conditions for this type of disruption have been discussed in a number of papers.[17,18] The currently accepted mechanism for this voltage range is that, provided there is no substantial release of gas due to electron bombardment of the anode causing a large increase in ambient pressure, disruption occurs when the hottest part of the cone approaches the melting point of the material of which it is composed. This is an unstable situation causing a runaway gasification of the tip analogous to an exploding wire. The temperature is governed by the heat-generating mechanisms of Joule heating and of the Nottingham effect,[19] and the heat-loss mechanisms of conduction down the shank and of radiation. The Nottingham effect tends to hold the emitting surface at a critical temperature T_c [20–23] where the energy lost to the surface by electrons tunneling from above the Fermi level is exactly balanced by the energy given up to the surface by electrons tunneling from below the Fermi level. To a close approximation T_c is given by

$$T_c = 5.32 \times 10^{-5} E/\phi^{1/2} \quad ^\circ\mathrm{K}. \tag{13}$$

The tips of TFFEC devices disrupt when the emission drawn from them is in the range 50—150 μA. If the larger area desired for the cone tip in Sec. III C is used, 50 μA corresponds to a current density of

$$J = (50 \times 10^{-6})/(6.3 \times 10^{-11}) = 8 \times 10^{5} \quad \mathrm{A/cm^2}. \tag{14}$$

This current density with a work function of 2.6 eV would require $E = 2.2 \times 10^{7}$ V/cm giving $T_c \sim 790\,^\circ$K. On the other hand, if the smaller area is used, the current density is

$$J = (50 \times 10^{-6})/(1.2 \times 10^{-15}) = 4.1 \times 10^{10} \quad \mathrm{A/cm^2}.$$

This current density and a work function of 4.35 eV would require $E = 15 \times 10^{7}$ V/cm giving $T_c \sim 3800\,^\circ$K. The surface is always at a lower temperature than T_c because of the dominant effect of conduction.[21] Thus, to account for tip disruption caused by melting, use of the smaller emitting areas with the high T is indicated, since the melting point of molybdenum is 2893 °K.

IV. EMISSION STABILITY

A. General background

Time variations of emission from a source can be divided into four classes as follows:

(a) A slow deterioration in the average emission characteristics that takes place over long periods of time. This limits the useful life of the cathode, which may be defined by some arbitrary factor such as the time for the average emission at a given voltage to decrease by a chosen amount. For use in a microwave tube, cathode lives of from 10 000 to 100 000 h may be desirable. In demountable electron optical devices such as a scanning electron microscope, cathode lives of a few hundred hours may be acceptable.

(b) A sudden increase or decrease of emission which then remains unchanged for periods of time from 10^{-1} to 10^{2} sec. These have been called "short-term fluctuations", and are observed mainly on the single-cone TFFEC's and the etched wires.

(c) A low-frequency noise containing frequencies in the range 10 Hz to 100 kHz. These fluctuations make up the "flicker" noise.

(d) The shot noise, which is directly related to the discrete nature of the electron and usually becomes dominant at frequencies above 100 kHz.

The single cones, the character of the flicker noise changes dramatically in bursts that last from 10^{-1} to 10^{2} sec. These bursts are usually associated with the change of emission noted in (b). For arrays the superposition of the burst noise from individual cones causes the burstlike characteristic to be substantially modified (measured as a fraction of the total current). In the 100-cone arrays bursts are rarely seen, and the effect is essentially nondetectable in the 5000-cone arrays.

In Sec. IV B, measurements on these effects are discussed in more detail.

B. Life

Five single-cone TFFEC's were put on life test in a 50-l/sec ion-pumped system at a pressure of more than 10^{-9} Torr. Each TFFEC was operated continuously at a current of 1 μA with a collector potential of 120 V. During the initial measuring period, the gate potential for 1-μA emission dropped until a steady value (around 120 V) was reached. The cathodes then continued essentially unchanged for 3300 h when the life test was terminated.

Life tests were also made with three of the 100-cone arrays. These data were obtained in sealed tubes with a 2-l/sec ion appendage pump as shown in Fig. 13. The tubes were processed before they were sealed as described in Sec. II, with a pressure in the tube of about 10^{-9} Torr, as measured at the appendage pump. An alternating potential at a frequency of 60 Hz was applied to the gate that, by its action, produced a rectified cur-

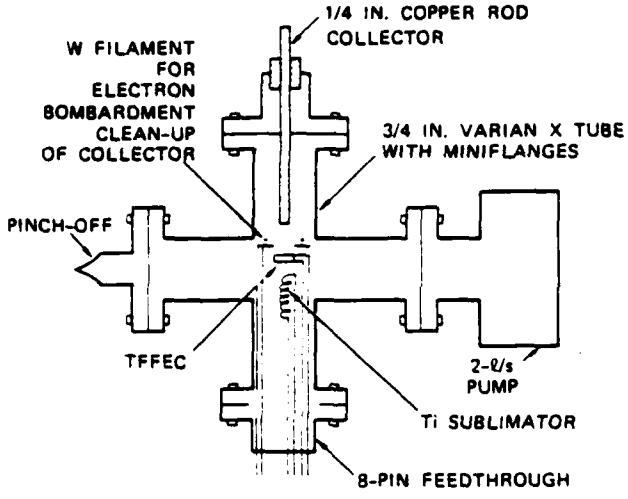

FIG. 13. Schematic of life test tube.

rent, thus reducing the anode dissipation. After an initial aging period of a few hundred hours the pressure reached a barely detectable level on the appendage ion pump, indicating a pressure of less than 10^{-9} Torr. The emission was held at a 2 mA peak corresponding to an average of 20 μA peak per cone and an overall peak current density of 3.2 A/cm². This was a stringent test, since the peak current per cone approached the disruption value. The results are shown in Fig. 14.

The collector power supply for each of the cathodes failed during the life test, causing the electron current to be collected by the thin molybdenum gate electrode. For two of the cathodes [see Figs. 14(a) and 14(b)] this event occurred early in life and both cathodes slowly but completely recovered from this experience over a period of about 1200 h of operation, indicating that the effect was most likely due to impurities released from the gate film being adsorbed on the cone tips rather than any changes in the geometry of the tips or the disruption of some of the cones, both of which would have caused a permanent change. Nevertheless both these cathodes showed evidence of a subsequent gradual decline of emission performance with time, amounting to about 10% in 7000 h of total life. The third [Fig. 14(c)] cathode had its anode supply fail after 4400 h of operation at which time it showed an erratic decline, but has remained stable at 1.2-mA emission for the last 1000 h. If Brodie's theory[3] of tip erosion by ion sputtering is applied, an approximate life of

$$L = \frac{2\times10^{-11}}{IP} = \frac{2\times10^{-11}}{(20\times10^{-6})(5\times10^{-10})} \approx 2000 \text{ h}$$

is obtained. This assumes a current of 20 μA per cone and a pressure of 5×10^{-10} Torr. This value of L is of the correct order of magnitude, bearing in mind that the ac voltage applied to the gate is rectified so that the cathode is actually operated for less than one-half the time.

On the other hand, the erratic decline for cathode 17-18-5E appeared to occur in steps, which argued that cone disruption in groups was taking place at the higher emission density per tip, at which this cathode was operating after the collector supply accident. For this reason, the gate voltage was reduced and although the total current was also reduced it has remained stable for a further 1000 h.

While much more work on cathode life is necessary before definitive conclusions can be made, lives of several thousand hours at overall emission densities of 3.2 A/cm² can be expected in good ion-pump vacua for the 100-cone TFFEC arrays.

Life tests on the 5000-cone arrays have been planned but no data are available at the time of this writing.

C. Short-term fluctuations

Figure 15 shows the types of short-term fluctuations typically observed with single-cone TFFEC devices, as recorded on a strip-chart recorder moving at the rate of 0.2 cm/sec. The cathode in this case was well aged by operating it for several hundred hours on a 500-l/sec ion-pumped system, which was monitored with a quadrupole mass spectrometer. During the entire experiment, the pressure was 10^{-10} Torr or better and the quadrupole showed that the residual gas was mainly

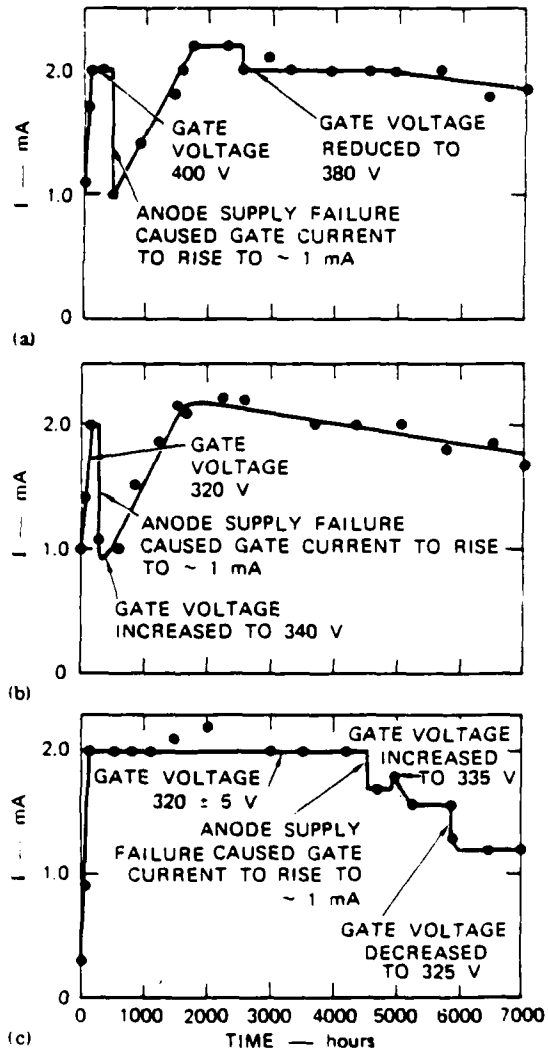

FIG. 14. Life test results: (a) cathode 17-13-17-D; (b) cathode 17-13-17-G; (c) cathode 17-18-5-E.

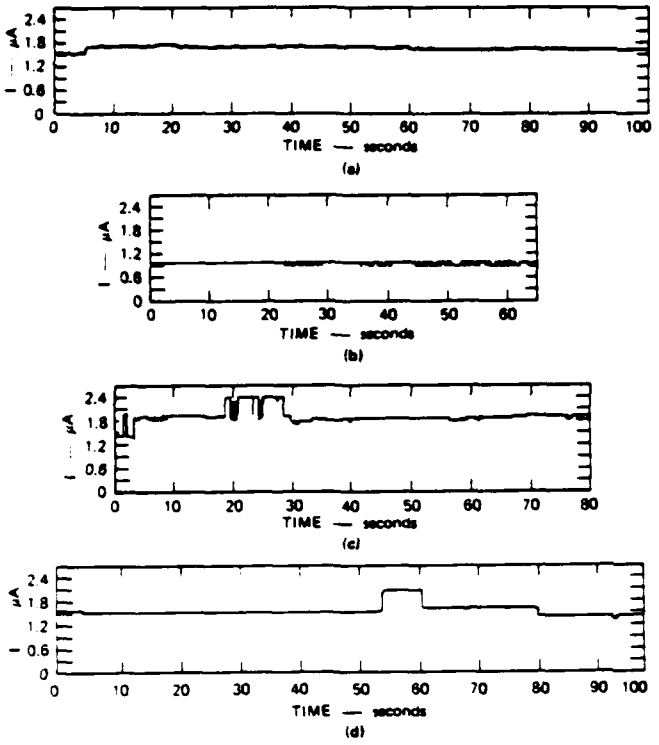

FIG. 15. Short-term fluctuations observed with single-cone TFFEC.

hydrogen. Nevertheless the current is rarely "steady", and is almost always showing bistable changes that appear to come in groups. The pulses within a group are usually of the same amplitude but the amplitude may vary from group to group. For example, in Fig. 15(c) where the average emission current was about 2 μA, large bistable changes of 0.5 μA or 25% of the average current were observed and lasted from 0.1 to 5 sec. A similar large-amplitude change is seen in Fig. 15(d). Figure 15(b) shows a clear bistable sequence of smaller amplitude 0.12 A at an average current of 1 μA, (i.e., a 12% fluctuation) that lasts from 0.1 to 2 sec. Note that even during the relatively quiescent period shown in Fig. 15(a), the changes are always in the form of steep sided steps (within the response time of the recorder.) Similar behavior is observed with the conventional etched point. With the 100- and 5000-cone arrays, the bistable character of the short-term fluctuations is lost and the variation of current with time has a more random appearance. Figure 16(a) shows a 100-cone array operating at 1 mA or 10 μA per cone; the rms deviation is about 1% indicating that the noise is caused by the fluctuations of individual cones, as is to be expected. For the 5000-tip array, the fluctuation of individual cones is always too small, compared with the total current, to be observed on this scale [Fig. 16(b)].

D. Burst noise

Burst noise has a waveform of bistable or multistable levels that can best be described as a nonstationary fluctuation superimposed on otherwise white noise.[24] It was first observed in the waveform of germanium point-contact diodes[25] and has subsequently been observed in tunnel diodes, resistors, forward- and reverse-biased p-n junctions, and junction transistors.[26]

Tunnel diodes are similar to the field emitters described in this paper, in that electrons are injected into the crystal lattice by field emission. In our field emitters, the electrons were injected into a vacuum and it was also found with the single-cone TFFEC's that bursts of bistable and multistable modes occurred. These bursts can usually be associated with the short-term fluctuations described above. The duration of a given burst can be from less than 1 sec to minutes, and the bursts can be followed by relatively quiescent periods within the same time range.

The noise bursts consisted of a series of current pulses, either positive or negative, superimposed on the constant operating current. The character of the pulse remains similar during a burst but sometimes varies from one burst to another. Observation of these pulses on an oscilloscope is limited by the time constant of the input circuit. In our initial experiments, this time constant was fairly large—on the order of 0.5 msec; this caused pulses of the form shown in Fig. 17(a). By using an FET source-follower amplifier, the input circuit time constant was reduced to less than 2 μsec. Oscillographs taken in this way [Fig. 17(b)] demonstrated that the pulses of Fig. 17(a) were actually composed of sequences of pulses of equal height whose duration varied from a value shorter than the new response time

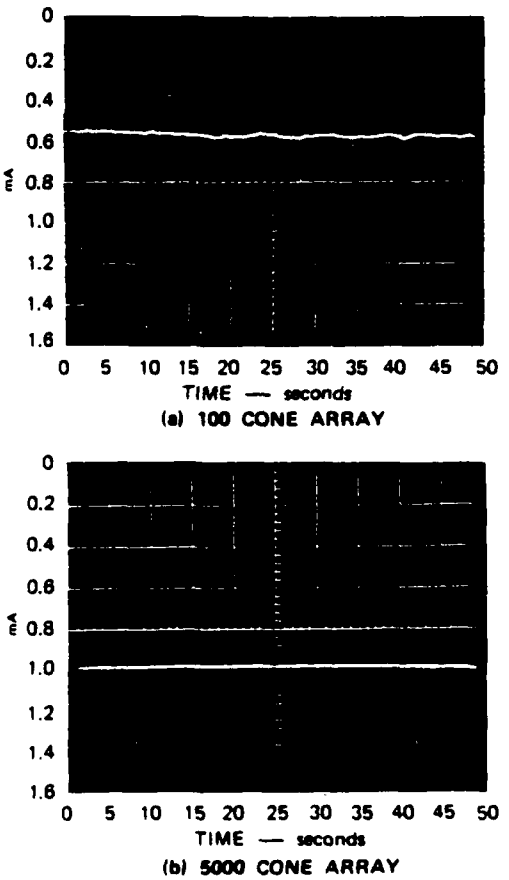

FIG. 16. Short-term current fluctuations from TFFEC array after 450°C bakeout and 100 h aging. (a) 100-cone array; (b) 5000-cone array.

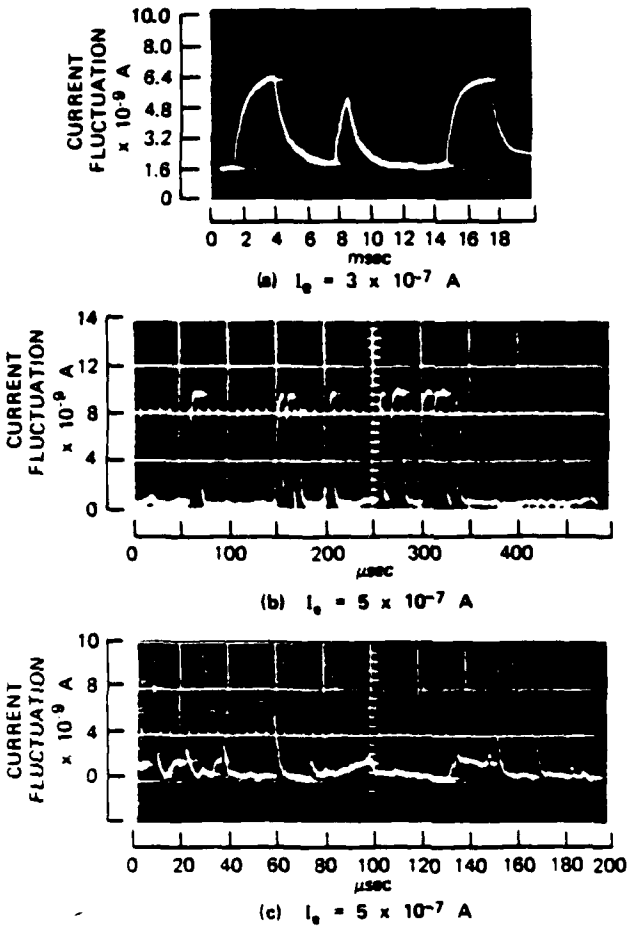

FIG. 17. Bursts of current pulses from single-cone TFFEC's.

(i.e., less than 2 μsec) to 20 μsec. These short pulses might consist of unresolved pulses of even shorter duration, but we have not been able to reduce the time constant further. These results were all obtained in the 500-l/sec ion-pumped system with well-aged cathodes operating in a vacuum of better than 10^{-10} Torr, the residual gas being mainly hydrogen.

The most striking facts about these bursts of pulses is that most are of equal height (or bistable) and come in groups, which can last for several milliseconds, although there is a random time distribution of pulses within the groups. Furthermore, the millisecond groups themselves come in bursts, with durations from fractions of a second to minutes.

When the amplitude of the basic (short) pulse is large but the duration of the pulse is less than the response time of the circuit, the pulse appears as a spike with a sharp front and a characteristic decay. The fact that the circuit has not fully responded means that the peak does not represent the full height of the pulse, and in certain modes, this effect causes the trace to have a more random appearance [Fig. 17(c)]. However, it seems likely that sufficient time resolution would show these pulses to be of equal height.

The superposition of the short pulses from individual cones makes the burst effect less distinctive in the arrays, although it is still observable. However, in this respect the etched wires behave similarly to the single cones.

E. Flicker noise spectra

Figure 18 gives a schematic diagram of the equipment used to measure the noise spectra in the range 100 Hz to 100 kHz. The cathodes were all operated in the 500-l/sec ion-pumped system described above at pressures below 10^{-10} Torr with the residual gas being mainly hydrogen. It was necessary to measure the noise output at the different frequency ranges contemporaneously to avoid the effects caused by sudden changes in noise properties, particularly those shown in the single-cone cathodes.

Eight fixed-frequency high-Q bandpass filters were constructed with center frequencies of 100, 250, 500,

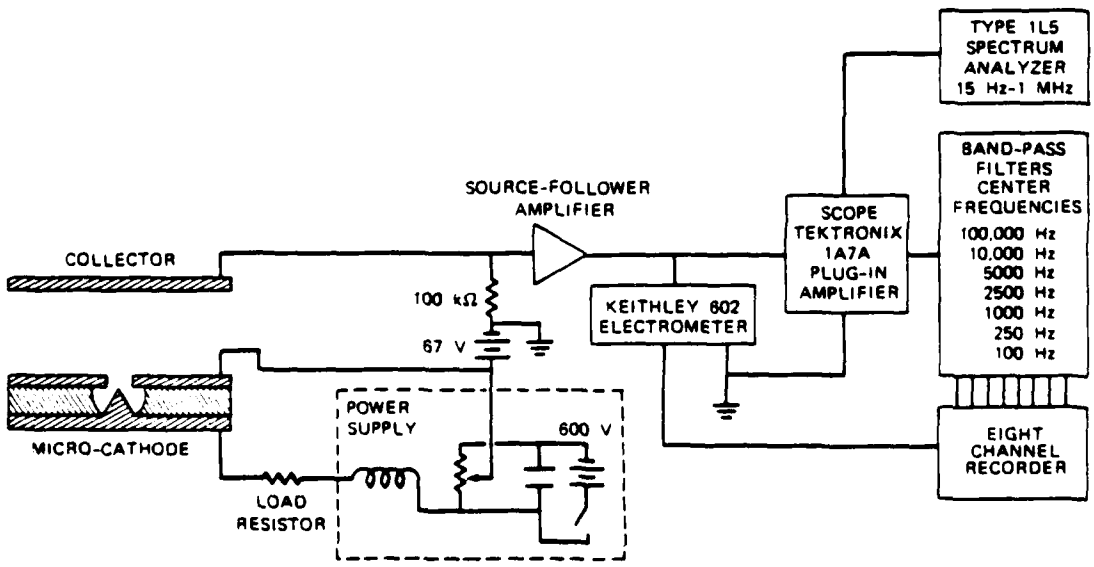

FIG. 18. Noise measurement system.

APP-I-12

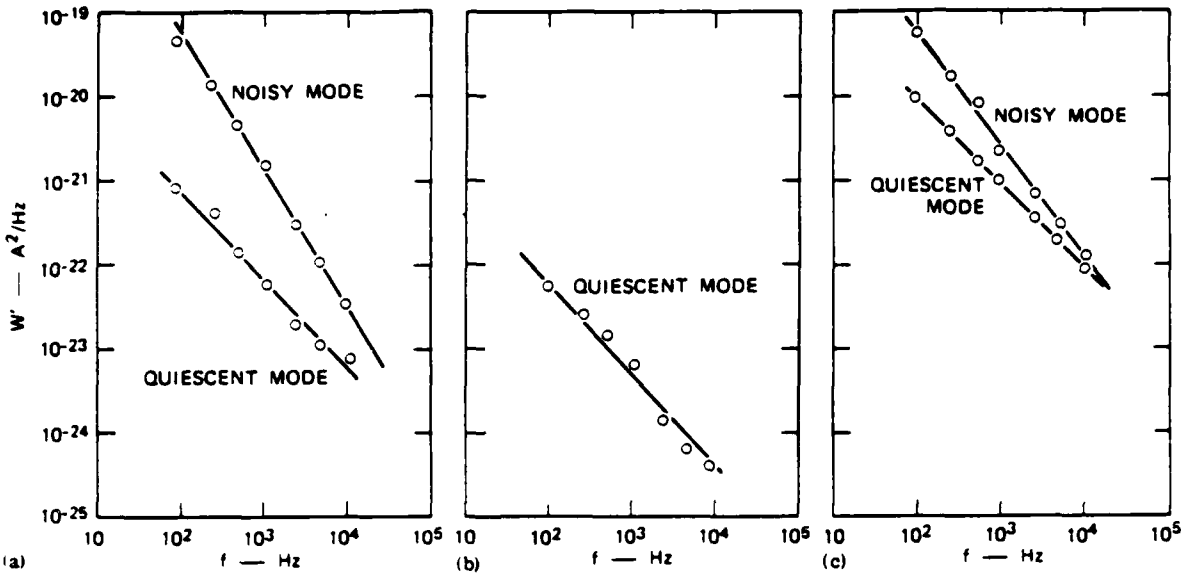

FIG. 19. Noise spectra for single-cone TFFEC (18-11-2T). (a) $I = 2\times10^{-7}$ A, W' for shot noise $(2eI) = 6.4\times10^{-26}$ A²/Hz; (b) $I = 4.5\times10^{-8}$, W' for shot noise $= 1.4\times10^{-26}$ A²/Hz; (c) $I = 1.5\times10^{-6}$, W' for shot noise $= 4.8\times10^{-25}$ A²/Hz.

1000, 2500, 5000, and 10 000 Hz. A Tektronix IL5 was used as the 100 000-Hz filter. In addition, a Tektronix IL5 spectrum analyzer was used for monitoring the overall spectral distribution. The output impedance of the measurement circuit was too high to achieve good frequency response above 5000 Hz. However, the addition of an FET source-follower amplifier placed between the collector and the noise measurement equipment extended the flat frequency response to 500 kHz. The output of each bandpass filter was fed into an averaging circuit with a time constant of 10 sec, then into a channel of an eight-channel recorder. The recorded signal was thus proportional to the average rms value of the signal at the frequency of the filter. The system was calibrated using a saturated thermionic diode as a shot noise source and checked using sine waves of known amplitude.

In general, the flicker noise is described by the mean square current fluctuation $\langle i_f^2\rangle_{\Delta f}$ at a given frequency f in a given frequency range Δf when held at an average current I.

In general

$$\langle i_f^2\rangle_{\Delta f} = A\,W(f, J)\Delta f \tag{15}$$

$$= W'(f, I)\Delta f, \tag{16}$$

where A is the emitting area, J is the average current density, and W is the noise intensity distribution function. The objective of the measurements is to obtain W as a function of f and J. As outlined in Sec. III C, the estimation of the emitting area is open to differing interpretations. For this reason, we use Eq. (16) for the empirical description of the flicker noise. Plots of W' versus f at various values of I are obtained for each cathode.

Results for the single-cone cathode (18-11-2T), used for the previously illustrated Fowler-Nordheim plot, are shown in Fig. 19. In general, the spectrum differs

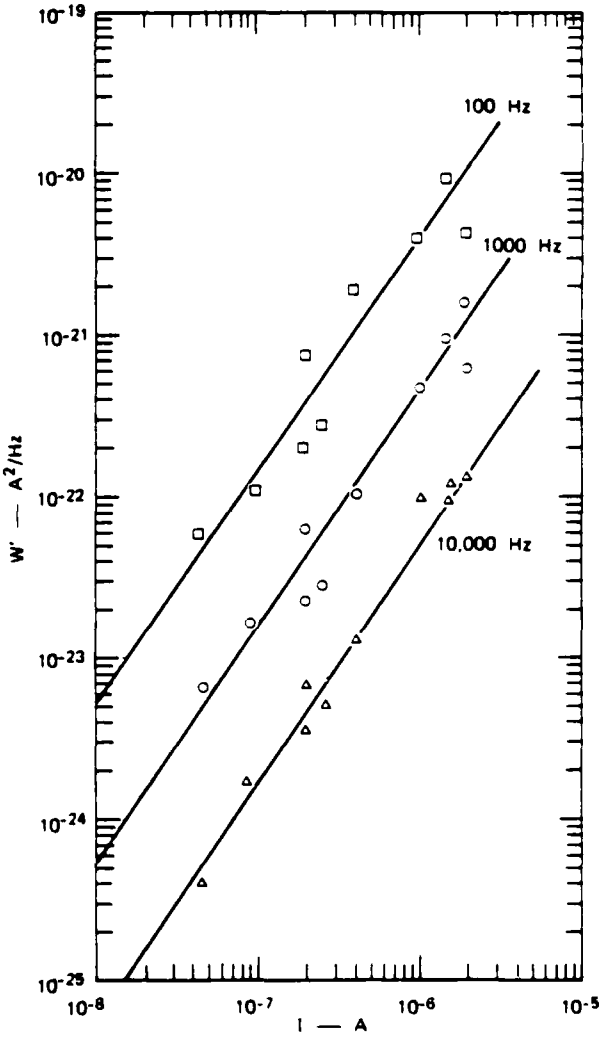

FIG. 20. Noise as a function of current for single-cone TFFEC in quiescent mode (18-11-2T).

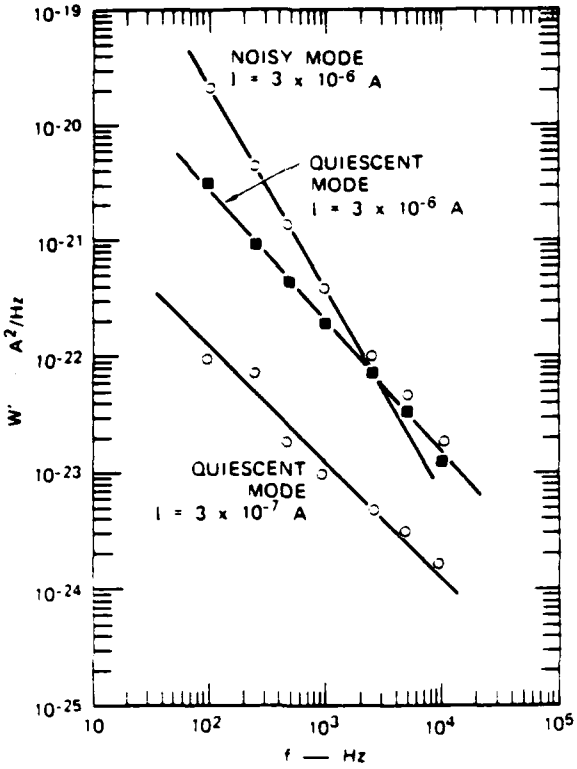

FIG. 21. Noise spectra for etched molybdenum points. (a) $I = 3\times10^{-6}$ A, (b) $I = 3\times10^{-7}$ A.

from mode to mode and the figure shows the spectra for the noisiest and the most quiescent modes at different current levels. Usually the most quiescent mode showed a spectrum close to $1/f$ and a current variation close to $I^{1.5}$ (Fig. 20). The noisiest mode showed a spectrum closer to $1/f^2$ and was not strongly dependent on the current over the measured range (4.5×10^{-8} to 1.5×10^{-6} A). The current range was bounded at the lower end by the sensitivity of the noise neasuring apparatus and at the high end by the desire to avoid any instabilities that might occur as the cone disruption current was approached.

The fact that the noise is not strongly dependent on the current in the noisiest mode is most extraordinary. The circuit was carefully checked to see that this noise was not being injected from some spurious source. Among other tests the field emission triode was replaced with a low-noise metal-film resistor to emulate the same operating conditions in the circuit. In the latter case, the noise was reduced to a very low level, and no evidence was observed to explain the existence of high noise bursts. Hence, we concluded that it was a genuine property of the field emitting source. Even in the "quiescent" mode, the flicker noise is many orders of magnitude above the shot noise in the frequency range measured for that current.

The etched molybdenum wire cathodes showed similar behavior (Fig. 21), with the noisiest mode roughly proportional to $1/f^2$ and the quiescent mode to $1/f$. The noisiest mode appeared to be somewhat quieter than the noisiest mode of the single cone and did not appear until currents of 5×10^{-7} A were drawn. For the quiescent mode, the noise versus current behavior (Fig. 22) is also similar to the single-cone TFFEC, being proportional to $I^{1.5}$ (Fig. 22) except that the noise from the etched wire is a factor of 10 smaller for a given current. If we use Eq. (1) to describe the noise and assume that the emitting surfaces are similar in both cases, we obtain

$$W_c' = A_c W(f, I/A_c) \tag{17}$$

and

$$W_E' = A_E W(f, I/F_E), \tag{18}$$

where c refers to the single-cone TFFEC and E to the etched molybdenum wire. If we further assume that $W\alpha(J^x/f^y)$, then

$$\frac{W_c'}{W_E'} = \frac{A_c}{A_E}\left(\frac{A_E}{A_c}\right)^x. \tag{19}$$

From the measurements shown in Fig. 22 we obtain $x = 1.5$, and $W_c'/W_E' = 10$, hence $A_E/A_c = 10^2 = 100$. This compares with a ratio obtained by the Fowler-Nordheim method (see Table I) for the same cathodes of 55. Bearing in mind the spread in the data from which these results were derived, agreement within a factor of 2 seems reasonable and supports the idea that the correct emitting areas are given by the Fowler-Nordheim method.

The spectra for the 100-cone arrays also show mode behavior, but the modes are not so sharply separable and exhibit curious spectra, as illustrated in Fig. 23. Presumably, each individual cone can be in a quiescent or noisy mode at different times, and the sum of the

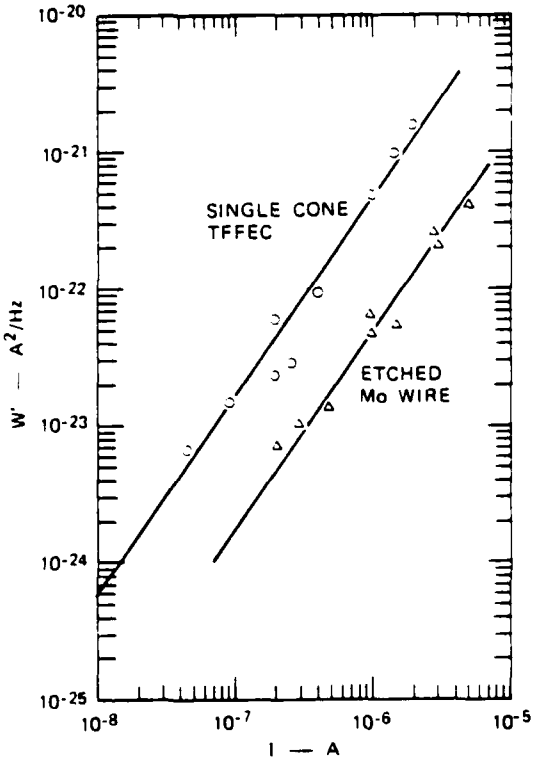

FIG. 22. Comparison of noise as a function of current at 1000 Hz for the single-cone TFFEC (18-11-2T) and the etched molybdenum point.

TABLE III. Comparison of flicker noise spectra for various field emission cathodes.

Cathode	Current range (A)	Frequency range	y	x	Ref.
Clean single-crystal tungsten	4.5×10^{-7} to 1.2×10^{-6}	100 Hz to 10 kHz	0.75	2	27
Tungsten with adsorbed residual gases	3.2×10^{-7} to 2.6×10^{-6}	100 Hz to 10 kHz	1—1.3	• • •	27
Tungsten with adsorbed barium	1.4×10^{-7} to 8×10^{-7}	100 Hz to 10 kHz	1.2—1.4	1	27
Tungsten with adsorbed potassium	6×10^{-7} to 2×10^{-6}	100 Hz to 10 kHz	1.2	1.86	29
Zr/W at 900—1576°K	10^{-8} to 10^{-7}	2—10 kHz	1—1.3	2.2	30
TFFEC molybdenum single cone (quiescent mode)	10^{-6} to 10^{-5}	100 Hz to 10 kHz	1	1.5	• • •
Etched molybdenum wire (quiescent mode)	10^{-7} to 10^{-5}	100 Hz to 10 kHz	1	1.5	• • •

noise currents from each is stationary for long enough to take a spectrum in a given condition. Figure 24 shows spectra for the 5000-cone array when operating at a current of 8.6×10^{-4} or 1.72×10^{-7} A per cone. Spectra were taken in the noisiest mode, in the quietest mode, and when elevated to a temperature of 275 °C. The character of the spectrum essentially remains the same regardless of its condition. Up to about 5000 Hz, the spectrum shows a $1/f^2$ characteristic. However, at around 5000 Hz, a new noise source, generated in the system, begins to become effective, which increases with increasing frequency, with a broad peak covering 50—100 kHz. Figure 25 shows that the current dependency of the noise in the $1/f^2$ portion of the spectrum is proportional to I, but proportional to I^2 at 100 kHz where the new noise source has become dominant. Note that there is no evidence for the existence of this new noise source in either the single- or 100-cone array. In the low-frequency half of the spectrum for the 5000-cone array, the total noise appears to be dominated completely by the cones in the noisy mode, since they always show a close to $1/f^2$ spectrum.

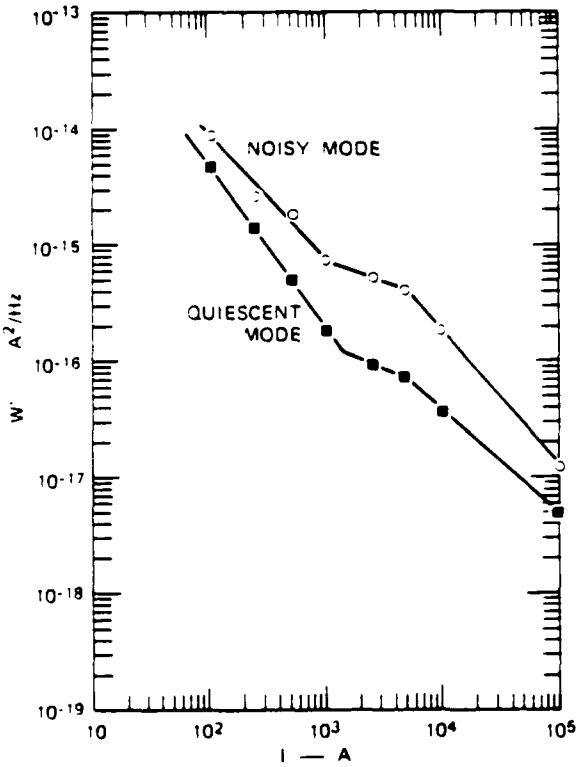

FIG. 23. Noise spectra for 100-cone array TFFEC (17-13-19F) at $I = 5.04\times10^{-4}$ A (where W' for shot noise $= 1.6\times10^{-22}$ A^3/Hz).

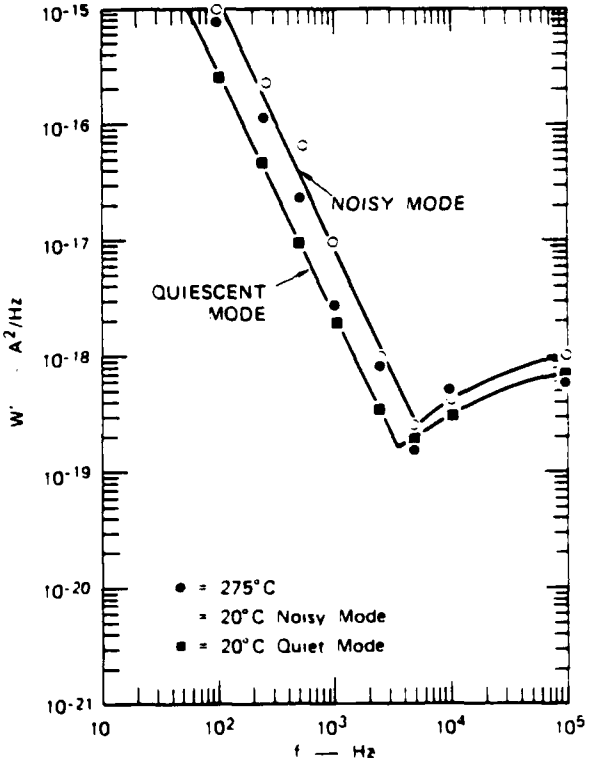

FIG. 24. Noise spectra for 5000-cone array TFFEC (20-6-1H) at $I = 8.6\times10^{-4}$ A (where W' for shot noise $= 2.75\times10^{-22}$ $A^2\cdot Hz$).

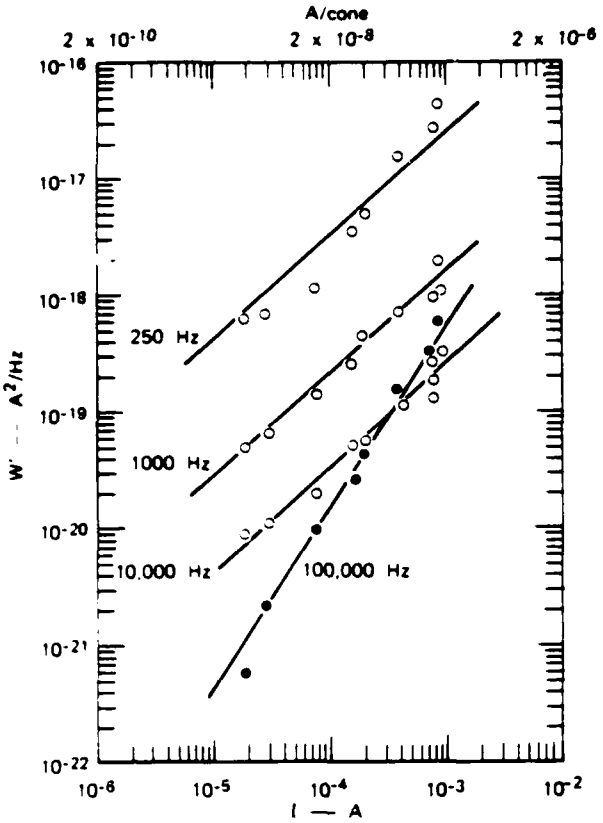

FIG. 25. Noise as a function of current for 5000-cone array TFFEC (20-6-1H).

In the case of the 5000-cone array, the difference in modes must be caused by the change in the number of cones in the noisy mode, since the contribution of the cones in the quiescent mode make a much smaller contribution to the total noise. The fact that the noise at a given frequency as a function of current shows a linear variation argues that the probability of the cone being in the noisy mode is proportional to the current being drawn from it. If all the cones were in the noisy mode at a level measured from the single-cone experiment, a saturation in noise would be expected when all the cones are in their noisiest state. Extrapolation of the data in Fig. 25 suggests that this would occur at about 3.5 mA when the noise would be 5000 times that of the single cone in its noisiest mode at a corresponding frequency. Unfortunately, the power limitation of the collector prevented these current levels from being reached on a continuing basis to check for this effect. However, at 2×10^{-7} A per cone the hypothesis suggests that about 30% of the cones are in the noisy mode at any given time, or each cone spends about one-third of its time in the noisy mode when drawing this current. Chart recordings of the single cone operating at 2×10^{-7} A showed that in a 300-sec (5-min) period it was in the noisiest mode for about 100 sec (comprised of three bursts each of approximately 30—40 sec duration). This result is consistent with the suggested explanation of the behavior of the 5000-cone array at the low-frequency end. The fact that the noise at the high-frequency end (100 000 Hz) increases as the square of the current demonstrates that its mechanism of generation is totally different from that at the low-frequency end of the spectrum.

Other investigators have studied field emission flicker noise,[27–30] but, unfortunately, none using molybdenum cathodes. No mention of the mode behavior reported here has been made even on contaminated points, and no data has been given from which the emission area could be estimated. However, the flicker noise showed the usual variations with frequency and current, when the shot noise had been subtracted, taking the form

$$\langle i_F^2\rangle_{av} \alpha I^x/f^y. \tag{20}$$

A comparison is given in Table III.

V. THE NATURE OF THE EMITTING SURFACE

The evidence given in this paper indicates that emission from the tip of the cones of the TFFEC arises from just one or a few atoms located on the tip. This evidence is summarized as follows:

(a) The areas given by the Fowler-Nordheim method are of the order of a few unit cell dimensions (Sec. III C).

(b) The electric fields at the tip, assuming a smooth spherical cap, are too small by a factor of 4 to account for the observed field emission without requiring an unreasonably low work function for the surface. The necessary enhancement factor is of the right order to be accounted for by an adsorbed molecule (Sec. III C).

(c) The apparent area reduction factor to be expected on the basis of a linear variation of work function with field is too large to be obtained without substantial deviation from the Fowler-Nordheim relationship. No such deviation is observed with the single-cone TFFEC (Sec. III C).

(d) Disruption of the cones at high current requires that the critical temperature of the Nottingham effect be above the melting point of molybdenum. This only occurs if the small areas given by the Fowler-Nordheim method is used (Sec. III E).

(e) The images observed in the field emission microscope for the single-cone TFFEC consists of one or a few "lobes" that show no regular pattern, as is usually observed with the larger single-crystal faces of conventional thermally grown points (Sec. II). The lobes are mobile. The resolution and interpretation of such lobes as images of atoms is consistent with work by Rose,[31] Becker[32] and others, as critically reviewed by Dyke and Dolan[33] and Good and Mueller[34]; and by studies of field emitting whiskers.[35]

(f) The equal heights and rapid rise times of the burst of current pulses in all the time domains studied (Secs. IV C and IV D) indicate the effect of single atoms, such as the rearrangement of atoms at the tip, the arrival and departure of atoms at the emitting area (by surface migration, solid diffusion from within the cone or arrival and departure to the vacuum external to the tip), or a change in the vibrational state of the adsorbed atom. The last change would alter the average distance from the surface of the adsorbed atom in a manner analogous to the nuclear separation of the diatomic

molecule and would thus cause a small local work-function change. The small-amplitude high-frequency pulses could arise from this source and the less common large-amplitude events from the gross movement of atoms from site to site.

(g) An alternative explanation worth discussing is the possibility that microneedles or whiskers are formed on the tips of the molybdenum cones similar to those recently reported by Okoyama,[36] who obtained dendritic growth on tungsten by the reduction of tungsten oxide. The dendrites were grown on 10-μ-diam tungsten wire; however, the ends of the whiskers were of similar dimensions to those of the cones grown in the experiments reported in this paper, having a tip radius of curvature in the range 0.05—0.2 μ. In other words, the tips of Okoyama's whiskers corresponded to the tips of the vapor-grown cones reported here. It seems unlikely that additional whiskers can grow from tips with radii of only 0.05 μ (or about 100 lattice spacings) since such whiskers would have to be only a few lattice spacings in diameter and a few atom spacings high to account for the observed field magnification factor. Thus, it would be a matter of semantics as to whether such protrusions were described as atomic bumps or whiskers. Considerable theoretical and experimental work has recently been done to explore the vibration spectra of adsorbed molecules by observing the energy distribution of field emitted electrons. A review of this technique called FEED has recently been given by Gadzuk and Plummer.[37] There can be no doubt as to the existence of an effect due to vibrational levels particularly at the temperatures that are likely to exist at the field emitting area.

Note added in proof. Life tests with the 100-cone arrays drawing 2 mA total emission (or 3 A/cm^2) have now continued in excess of 12 000 h as of October 1976.

ACKNOWLEDGMENTS

The work reported in this paper was done with support from the U.S Army Research Office, Durham, N.C., under Contract No. DAHC04-73-C-0007, and from the National Aeronautical and Space Agency, Lewis Research Center, Cleveland, Ohio, under Contract No. NAS3-18903. The work reported in this paper has benefitted from discussions and inputs from other past and present colleagues of the SRI Physical Electronics Group. The authors particularly wish to thank John Kelly for valuable discussions on the noise studies and for preparing the computer programs used in Sec. III E and Clifford C. Hartelius for advice in the materials science field. The field emission devices could not have been made without the outstanding microfabrication, design, and constructional skills of Robert D. Stowell and the diligent technical assistance of Hazel Pakka and Earl Heydon.

[1]C.A. Spindt, IEEE Conf. on Elec. Devices and Tech., New York 1973 (unpublished).
[2]C.A. Spindt, K.R. Shoulders, and L.N. Heynick, U.S. Patents 3,755,704 (1973), 3,789,471 (1973), 3,812,559 (1974).
[3]I. Brodie, Int'l J. Electron. 38, 541 (1975).
[4]A.H.W. Beck, Proc. IEE 106B, 372 (1959).
[5]A.S. Grove, *Physics and Technology of Semiconductor Devices* (Wiley, New York, 1967), p. 22.
[6]W.S. De Forest, *Photoresist* (McGraw-Hill, New York, 1975), p. 223.
[7]L. Heynick, E.R. Westerberg, C.C. Hartelius, Jr., and R.E. Lee, IEEE Trans. Electron Devices ED-22, 400—409 (1975).
[8]R.H. Fowler and L.W. Nordheim, Proc. R. Soc. London A 119, 173 (1928).
[9]R.E. Burgess, H. Kromer, and J.M. Houston, Phys. Rev. 90, 515 (1953).
[10]A. Van Oostrom, J. Appl. Phys. 33, 2917 (1962).
[11]E.M. Charbonnier and E.E. Martin, J. Appl. Phys. 33, 1897 (1962).
[12]W.P. Dyke and W.W. Dolan, Adv. Electron. Electron Phys. 8, 180 (1956).
[13]I. Brodie, J. Appl. Phys. 35, 2324 (1964).
[14]M. Abon and S.J. Teichner, Nuovo Cimento Suppl. 5, 321 (1967).
[15]G.A. Haas, *American Institute of Physics Handbook*, 3rd ed. (McGraw-Hill, New York, 1972), pp. 9—172.
[16]R. Gomer, *Field Emission and Field Ionization* (Harvard University Press, Cambridge, Mass., 1961).
[17]D. Alpert, P.A. Lee, and H.E. Tomasche, J. Vac. Sci. Technol. 1, 34 (1964).
[18]P.S. Chatterton, Proc. Phys. Soc. London 88, 231 (1966).
[19]W.E. Nottingham, Phys. Rev. 59, 907 (1941).
[20]P.H. Levine, J. Appl. Phys. 33, 582 (1962).
[21]I. Brodie, Int. J. Electron. 18, 223 (1965).
[22]F.M. Charbonnier, R.W. Strayer, L.W. Swanson, and E.E. Martin, Phys. Rev. Lett. 13, 397 (1964).
[23]D.A. Lee, University of Illinois Coordinated Science Laboratory Report R-280, 1966 (unpublished).
[24]W.H. Card and A. Mavretic, Second Symp. on the Physics of Failure in Electronics Chicago, 1963, Vol. 2, p. 268 (unpublished).
[25]R.G. Pay, thesis (University of Birmingham, 1956) (unpublished).
[26]S.T. Hsu, R.J. Whittier, and C.A. Mead, Solid-State Electron. 13, 1055 (1970).
[27]G.W. Timm, and A. Van der Ziel, Physica 32, 1333 (1966).
[28]Ch. Kleint, Surf. Sci. 25, 394 (1971).
[29]Ch. Kleint, R. Meclewski, and R. Blaszczyszyn, Physica 68, (1973).
[30]L.W. Swanson and N.A. Martin, J. Appl. Phys. 46, 2029 (1975).
[31]D.J. Rose, J. Appl. Phys. 27, 215 (1956).
[32]J.A. Becker, Bell Syst. Tech. J. 30, 907 (1951); J.A. Becker and R.G. Brandes, J. Appl. Phys. 27, 221, (1956).
[33]See Ref. 12, pp. 132—137.
[34]R.H. Good and E.W. Mueller, *Handbuch der Physik* (Springer-Verlag, Berlin, 1956), Vol. 21, p. 176.
[35]I. Brodie, J. Vac. Sci. Technol. 2, 249 (1965).
[36]F. Okuyama, J. Vac. Sci. Technol. 12, 1399, (1975).
[37]J.W. Gadzuk and E.W. Plummer, Rev. Mod. Phys. 44, 487 (1973).

APPENDIX II

The analysis of beam optics was done by STAR Microwave Consultant, J.M. Baird of The University of Utah. The approach was to use a best case/worst case analytical solution of the parallel plan approximation to the actual geometry (no hole in the anode). This was then used to define the geometry to be studied numerically using an electron gun computer code.

The computer solution appears as Figure 6 to this Appendix. It is based on an assumed distribution of emitted current as follows:

Emission Half Angle	% of Total Current Enclosed
0°	80
$\pm 30^{\circ}$	5,5
$\pm 45^{\circ}$	5,5

The resulting plot shows that current with 30° half angle would pass through the anode, while current with 45° half angle would be partially intercepted. Unfortunately, the chip which reached final test failed catastrophically before anode interception could be measured for verification.

BEAM SIZE ANALYSIS IN THE SPINDT CATHODE SPACE-GUN

J. M. Baird, University of Utah
for Star Microwave Inc.
December 1985

I. Intoduction

This report gives the results of calculations aimed at determining the beam expansion between the cathode and the anode of the Star Microwave "space-gun" which utilizes the new field emission Spindt cathodes. This gun has the design goal of achieving an average current density of 1 A/cm^2 from an array of 21 Spindt cathode elements spaced in an array covering a chip area of about 1 cm^2 as shown in **Figure 1**.

Each of the 21 cathode elements contains an array of 5000 point field emitters. These micoscopic field emitting diodes have a characteristic angular spread in their emission of about 30 degrees. Although there is no distinct beam boundary, it is believed that approximately 90% of the current falls inside this angular envelope. We have used the angle of 30 degrees to define a beam edge for the overall emission from each of the 21 cathode elements.

The Spindt cathode elements emit the desired current levels at about 100 volts and it is therefore necessary to place an accelerating anode over the Spindt array chip to increase the beam voltage to the final design value of about 1000 volts. To form a useful electron beam, this second anode must have an array of 21 holes which are centered over the Spindt cathode elements to allow the accelerated beamlets to pass through.

The aim of the analysis reported here is to determine of the size of the holes in the accelerating anode which will allow a high percentage of the beam to pass through. The approach used is to determine the beam expansion between the surface of a Spindt cathode element and the accelerating anode as a function of gap spacing, and thereby provide a basis for making a judicious design choice for both the spacing and the hole size.

The geometry of the Spindt element beamlet which is analyzed is shown in **Figure 2**. For the first order calculations given here, a laminar flow beam

is assumed to leave the cathode element with an initial edge ray angle Θ_1=30°, and to be accelerated across the gap under the influence of both E_r and E_z electric fields as illustrated in the figure. The strength of these fields depends on the assumed level of space-charge and the applied potential across the accelerating gap.

A first order analysis for design purposes comes from examining the two extremes of beam expansion. In the **worst case**, E_r is assumed to have the maximum possible value while E_z is assumed to have the minimum possible value near the cathode. To make this case readily solvable, we have assumed that the full space-charge in the beam can be attributed to each component of the field separately. This over-estimate will certainly give an absolute upper bound on the beam size at the anode. In the **best case** analysis, the space-charge is totally neglected. This makes E_r=0, and maximizes the accelerating influence of E_z*. The resulting beam edge trajectory gives an absolute lower bound on the beam size at the anode.

The results of these best and worst case solutions show that for cathode-anode spacings on the order of 0.040 inches or smaller, the two absolute bounds are close enough together to provide a basis for making some initial design choices.

The remainder of this report gives the details of this best and worst case analysis.

---

* Although E_z near the anode is actually lower under the zero-space-charge assumption, it can be shown that its increased value in the cathode region where the beam is moving more slowly reduces the transit time across the gap and therefore minimizes beam spread.

II. Theory Used for Beam Edge Spreading Calculations.

The velocity of the edge-ray electrons is governed by the force equation

$$\frac{d\vec{v}}{dt} = \eta \vec{E} \qquad (1)$$

where **v** is the velocity vector, **E** is the electric field vector, and $\eta = q/m$ is the charge to mass ratio which is negative for electrons. In cylindrical coordinates with angular symmetry **Equation 1** becomes

$$\frac{dv_r}{dt} = \eta E_r$$
$$\frac{dv_z}{dt} = \eta E_z \qquad (2)$$

where

$$\frac{dr_b}{dt} = v_r$$
$$\frac{dz}{dt} = v_z \qquad (3)$$

define the radial and longitudinal velocities in terms of the time derivatives of the edge ray position (r_b,z).

It is useful to change independent variables by $dt = dz/v_z$ to get

$$\frac{dv_r}{dz} = \frac{\eta E_r}{v_z}$$
$$\frac{dv_z}{dz} = \frac{\eta E_z}{v_z} \qquad (4)$$
$$\frac{dr_b}{dz} = \frac{v_r}{v_z}$$

The presence of v_z in the denominators on the right hand side of these equations does not present a problem for our analysis because the initial velocities of electrons leaving a Spindt cathode are never zero.

There are two sources of electric field to accelerate the beam in **Equations 4**. The first is the potential rise across the cathode-anode gap, $V_g = V_2 - V_1$. The second is the space-charge in the beam. Poisson's

Equation describes how the electric field components change due to space-charge.

$$\nabla \cdot \vec{E} = \frac{\rho}{\epsilon_o}$$

or

$$\frac{\partial E_r}{\partial r} + \frac{\partial E_z}{\partial z} = \frac{\rho}{\epsilon_o} \qquad (5)$$

For our purposes, there is no simple way to analytically determine E_r and E_z for the proposed geometry, but we can look at two extreme cases which produce bounding limits on the value of r_2 (the radius of the edge ray at the anode) and thereby bracket the desired solution.

A maximum bound for r_2 will occur when E_r is maximum and E_z is such that the electron takes the longest possible time to cross the gap. An absolute maximum value for E_r comes from attributing all of the space-charge in **Equation 5** to the $\partial E_r/\partial r$ term. **Equation 5** then becomes

$$\frac{\partial E_r}{\partial r} = \frac{\rho}{\epsilon_o} \qquad (6)$$

which can be integrated to give

$$E_{r\,(max)} = \frac{I_o}{\pi \epsilon_o r_b V_z} \qquad (7)$$

where we have used $\rho = I_0/(\pi r_b^2 v_z)$ and I_0 is the total element current (which is negative for an electron beam). **Equation 7** gives the usual electric field used to determine the "universal beam spread curve"; i.e., the edge trajectory of a uniform laminar flow beam as it moves under the influence of its own space-charge. This is the maximum possible E_r and certainly represents a large over-estimate when $d \leq 2r_1$ in which case the two electrodes are close enough together to partially shield the beam edge from the effects of the space-charge in the central part of the beam.

It can be shown that the $E_z(z)$ associated with the maximum possible transit time is one in which its value at the cathode, E_1, is minimum. The deepest possible reduction of E_z at the cathode can be found by associating all of the space-charge in **Equation 5** with the E_z term. This leads to

$$\frac{\partial E_z}{\partial z} = \frac{\rho}{\epsilon_o} \tag{8}$$

If we were to assume that current density J ($=\rho v_z$) is a constant along with $\phi(0) = V_1 = 0$, and $E_z(0) = 0$, this would lead to the standard space-charge limited flow in a planar diode which gives $E_z(z) \propto z^{1/3}$. Since our beam does expand, however, so that $J=J(z)$ is not a constant, and since V_1 is not zero for the Spindt cathode injected beam, we must numerically integrate **Equation 8** to obtain quantitative results. If we combine **Equation 8** with **Equations 4** and add the definition of potential, $E = -\nabla\phi$, the result is a set of five first order differential equations in five unknowns (r_b, v_z, v_r, ϕ, E_z). Once again we use $\rho = I_0/(\pi r_b^2 v_z)$ (where I_0 is a constant and r_b and v_z are treated as functions of z) to get

$$\begin{aligned}
\frac{dr_b}{dz} &= \frac{v_r}{v_z} \\
\frac{dv_z}{dz} &= \frac{\eta E_z}{v_z} \\
\frac{dv_r}{dz} &= \frac{\eta I_o}{\pi \epsilon_o r_b v_z^2} \\
\frac{d\phi}{dz} &= -E_z \\
\frac{dE_z}{dz} &= \frac{\eta I_o}{\pi \epsilon_o r_b^2 v_z}
\end{aligned} \tag{9}$$

This set of equations forms a closed set which can be numerically

integrated over the interval $0 \leq z \leq d$ using the five known boundary conditions

$$\begin{aligned} \Phi(0) &= V_1 \\ \Phi(d) &= V_2 \\ v_r(0) &= v_0 \sin(\theta_1) \\ v_z(0) &= v_0 \cos(\theta_1) \\ r_b(0) &= r_1 \end{aligned} \tag{10}$$

where v_0 is determined from the initial energy $eV_1 = mv_0^2/2$.

Note, however, that this is not a simple initial value problem. Since the equations are nonlinear, this requires that a search be made for the proper initial condition $E_z(0) = E_1$ which corresponds to the desired downstream boundary condition $\Phi(d) = V_2$.

This search for the initial value of E_z was handled as follows. We assume that $\Phi(d)$ is implicitly a function of the initial condition E_1 and we expand in a Taylor's series about the desired point

$$V_2 = \Phi(d,E_1) = \Phi(d,E_{10}) + \Delta E_1 \left.\frac{\partial \Phi}{\partial E_1}\right|_{d,E_{10}} \tag{11}$$

where $E_1 = E_{10} + \Delta E_1$. We can then solve **Equation 11** for E_1 to get

$$\Delta E_1 = \frac{V_2 - \Phi(d,E_{10})}{\left.(\partial \Phi/\partial E_1)\right|_{d,E_{10}}} \tag{12}$$

Equation 12 is used to numerically estimate a correction ΔE_1 which when added to the initial condition E_{10} will make $\Phi(d)$ move closer to the desired value of V_2. When this algorithm is applied iteratively, the initial condition E_1 converges to the desired value.

The definition of the derivative was used to numerically estimate a value for $(\partial\Phi/\partial E_1)=\Phi_E$.

$$\Phi_E \equiv \left.\frac{\partial\Phi}{\partial E_1}\right|_{d,E_{1a}} = \frac{\Phi(d,E_{1b}) - \Phi(d,E_{1a})}{E_{1b} - E_{1a}} \qquad (13)$$

where $(E_{1b} - E_{1a})$ is made numerically small. This numerical procedure worked well for values of $d \geq 2r_1$ where rapid convergence to a fractional error of 10^{-4} was obtained. For $d < r_1$ convergence was slower but still obtainable down to $d = r_1/2$.

III Design Trade-off Calculations

A fourth order Runge-Kutta method was used for the numerical integration of **Equations 9** across the gap. The physical parameters used in these calculations were as follows:

V_1 = 100 Volts (injection potential at the cathode)

V_2 = 1000 Volts. (accelerating potential)

Θ_1 = 30 degrees (initial beam edge angle)

r_1 = 0.5 mm (Spindt cathode element radius)

I_0 = -49.16 ma (element current to give - 1A/cm^2 overall average current density from the chip)

The initial guess for the value of E_1 was the field in the gap in the absence of space-charge (i.e., $E_{10} = -(V_2-V_1)/d$) and the correction procedure defined by **Equations 12 and 13** was used to iterate E_1 until the *boundary condition* $\phi(d) = V_2$ was satisfied.

To determine the edge-ray trajectory for the **best case**, the current I_0 was set equal to zero. This is equivalent to neglecting all space-charge in the beam so that the edge-ray trajectory is the same as that of a single ballistic electron traversing the gap with the edge-ray initial conditions. In this case, there is no need to search for the E_1 boundary condition because the initial guess is the desired value.

The results of these calculations are shown in Figures 3 through 5. **Figures 3 and 4** show the best and worst cases of edge ray spreading as the beam moves across the gap. These two figures pertain to gap spacings, d, of 0.040 inches and 0.080 inches respectively and the plots are normalized to these values. These figures show the typical data obtained from solutions at any specific gap spacing.

Figure 5 presents a summary of ten different cases of gap spacing. In this figure the value of $2r_2$ (the <u>diameter</u> of the beamlet at the anode) is plotted versus the cathode-anode spacing. Here all quantities are plotted

in inches. Note in **Figure 5**, that the worst and best cases of beam spreading are fairly close together for gap spacing up to 0.040 inches. In this range a very reasonable estimate of the required anode hole size can be obtained.

<u>If we choose 0.040 inches for the gap spacing, a reasonable value for the anode hole diameter from Figures 3 and 5 is about 0.065 inches.</u>

This estimate is closer to the best case than to the worst because it is believed that the worst case for this gap spacing has the largest error. This is because the gap spacing and the Spindt element diameter are approximately the same size and the electrodes in this case will tend to shield the edge ray from the effects of space-charge in the central portion of the beam; i.e., tend to "short out" the radial E_r-Field.

IV. Conclusions and Recommendations.

A first order calculation has been made which shows that an anode hole diameter of about 0.065 inches with a cathode-anode spacing of 0.040 inches will provide a reasonable starting point for design of the Spindt cathode space-gun.

To help eliminate the uncertainty in the anode hole size we are pursuing a much more elaborate numerical simulation of this design at the present time. This simulation is being done using an established 2-D computer gun code in which the emission from the Spindt array elements can be simulated by multiple electron rays launched at a variety of angles from each emission point on the cathode. In addition, we are using a realistic anode hole boundary which will show how the anode hole affects the beam spreading and interception.

This type of simulation provides the very best analysis and design tool available provided that the distribution of velocities from the Spindt cathode are known. At the present time, however, the uncertainty of this velocity distribution will severely limit the ability of these gun simulations to predict the actual values of beam interception to be expected.

It is strongly recommended that a effort be made to experimentally determine the velocity distribution of electrons which are emitted from a Spindt field emission diode.

One method of accomplishing this measurement would be to have a Spindt cathode fabricated with only one emission diode (or several widely spaced diodes) and then to make beam analyzer measurements of the spatial distribution of the electrons emitted. It is recommended that this be done so that future applications of Spindt cathodes can have a firm basis from which to carry out computer simulations.

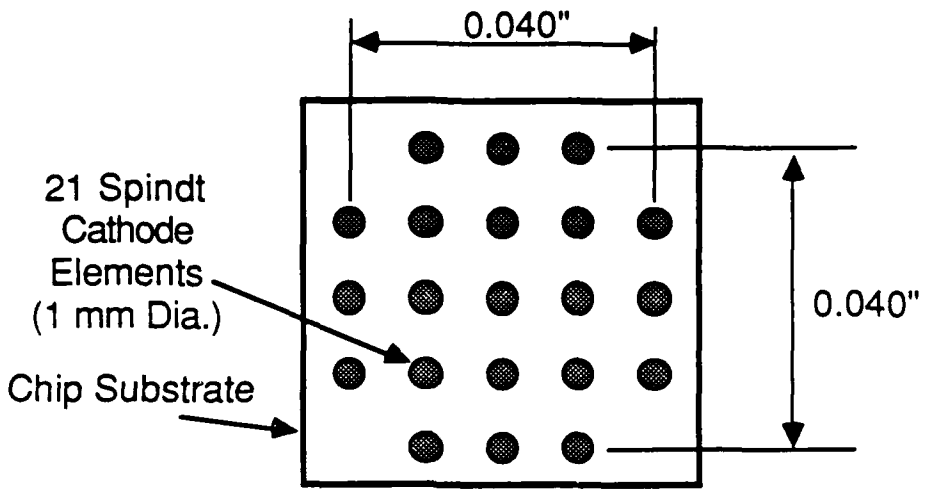

Figure 1. Overall geometry of the Spindt cathode chip with 21 cathode elements each of which contains a microscopic array of 5000 field emission diodes.

Model used for analysis of best and worst cases of beam edge ray expansion

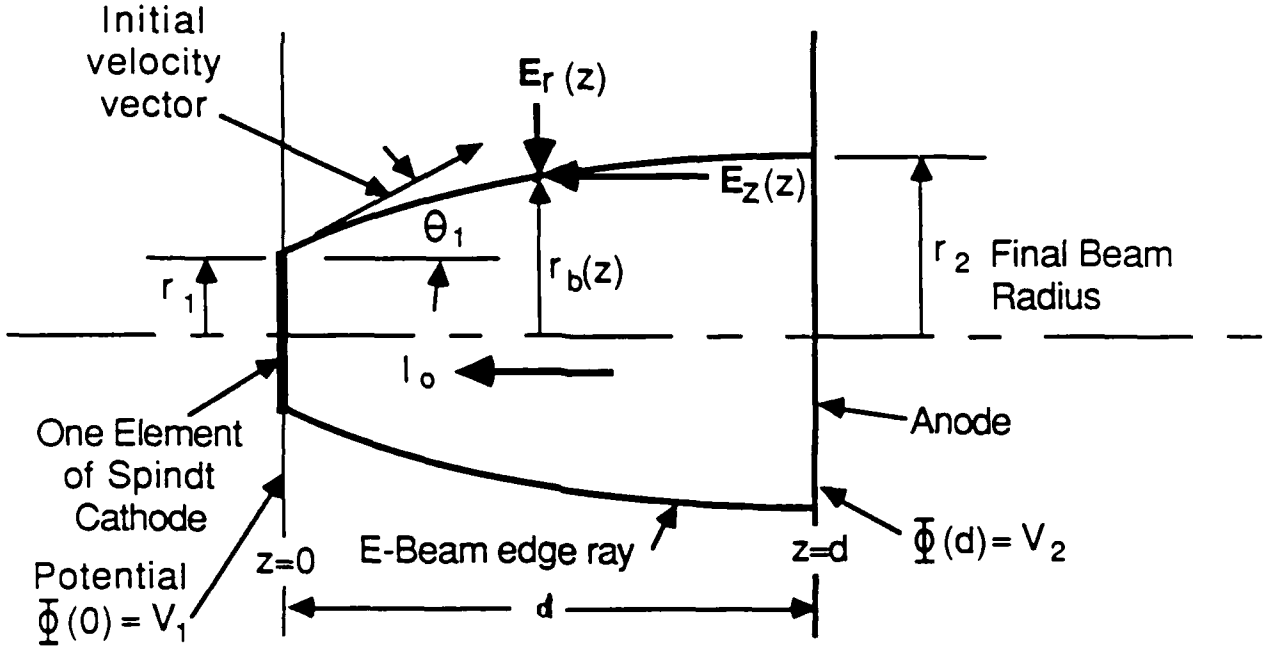

Figure 2. Geometric model of Spindt element and electron beamlet used for analysis.

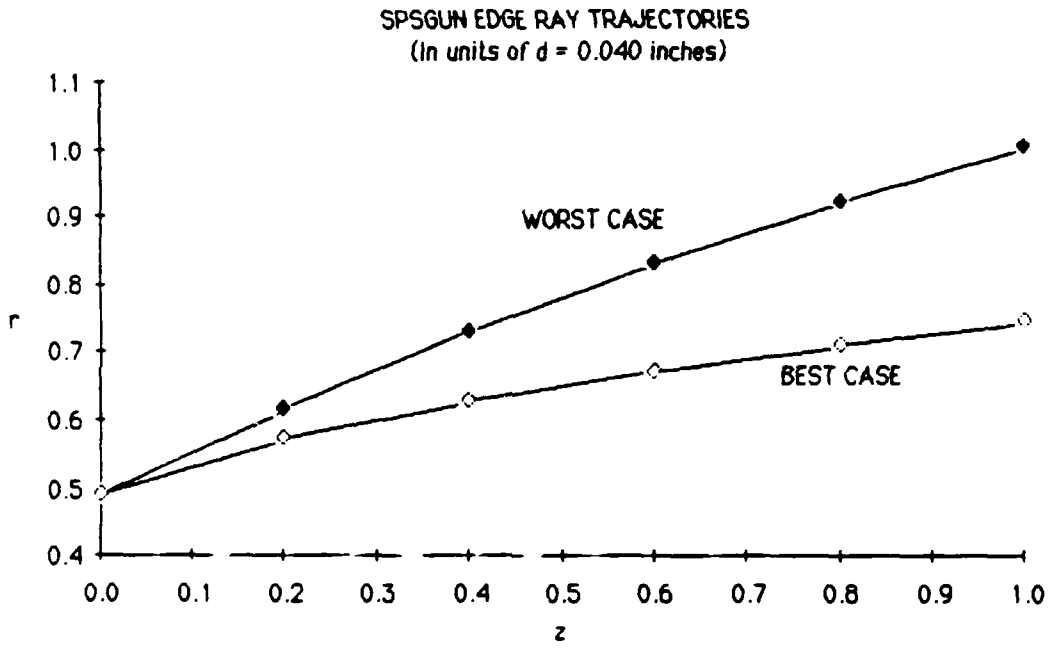

Figure 3 Best and worst case trajectories for a cathode-anode spacing of d = 0.040 inches

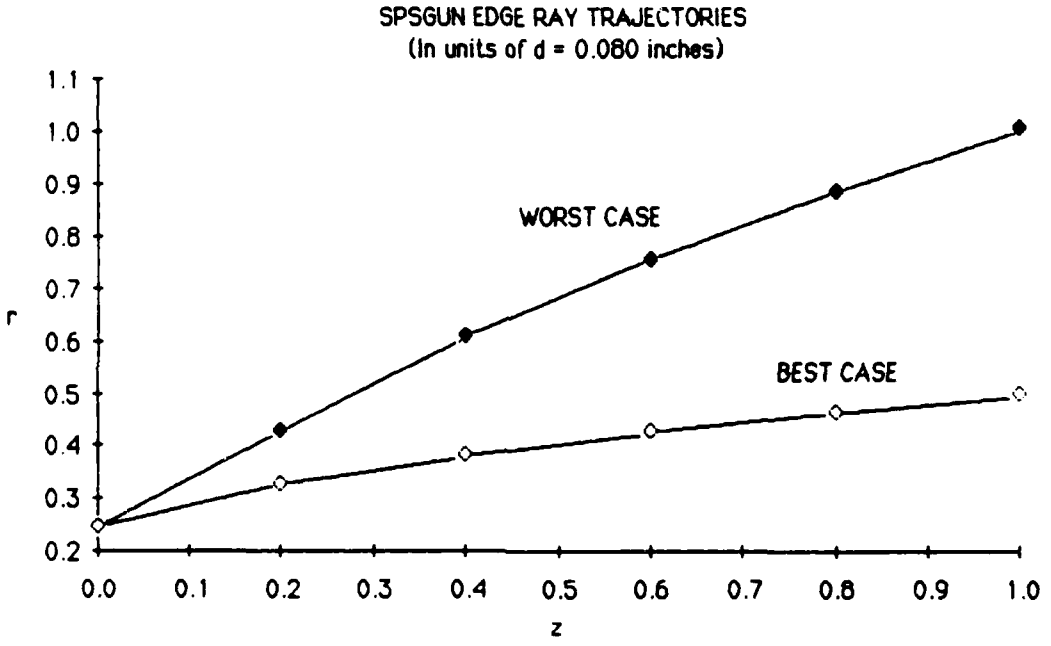

Figure 4 Best and worst case trajectories for a cathode-anode spacing of d = 0.080 inches

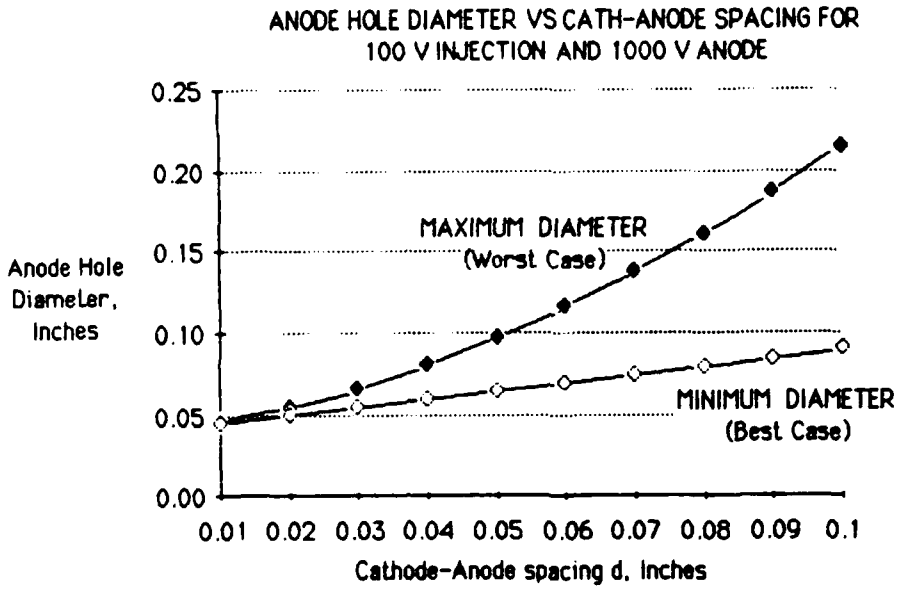

Figure 5. Anode hole diameter versus cathode-anode spacing, d, for the best and worst case trajectories.

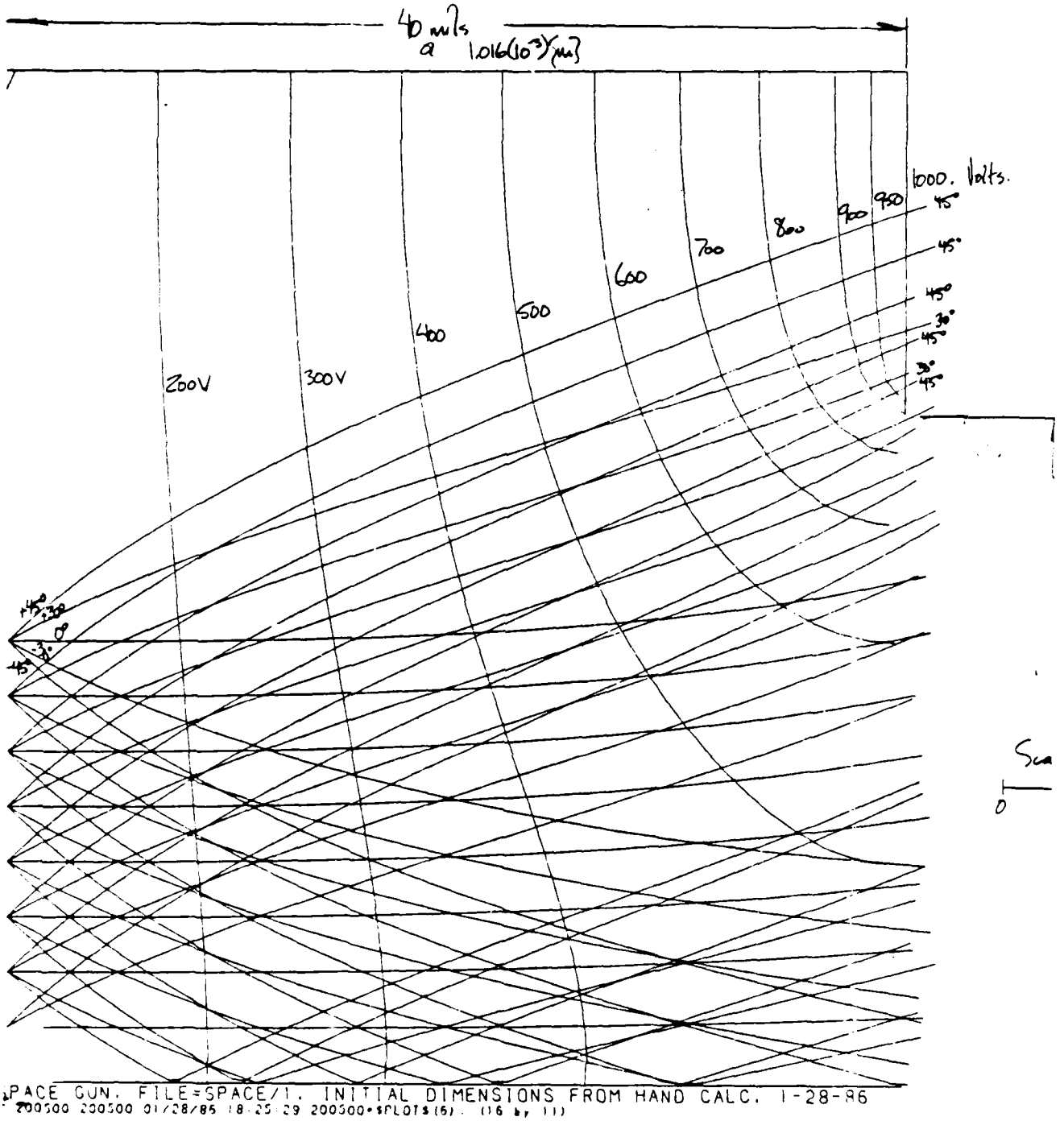

Figure 6: Computer Plot of Current From Field Emitter Spaced .040 From Anode With .062 Diameter Hole in Anode. Plot Shows That a .080 Would Have Passed All Current Emitted With Less Than 30° Half Angle.

MISSION
of
Rome Air Development Center

RADC plans and executes research, development, test and selected acquisition programs in support of Command, Control Communications and Intelligence (C^3I) activities. Technical and engineering support within areas of technical competence is provided to ESD Program Offices (POs) and other ESD elements. The principal technical mission areas are communications, electromagnetic guidance and control, surveillance of ground and aerospace objects, intelligence data collection and handling, information system technology, solid state sciences, electromagnetics and electronic reliability, maintainability and compatibility.

Printed by
United States Air Force
Hanscom AFB, Mass. 01731

END

DATE

3-88

DTIC